SIAM J. APPLIED DYNAMICAL SYSTEMS
Vol. 4, No. 1, pp. 101–139



# Existence and Bifurcation of Canards in $\mathbb{R}^3$ in the Case of a Folded Node*

Martin Wechselberger†

**Abstract.** We give a geometric analysis of canards of folded node type in singularly perturbed systems with two-dimensional (2D) folded critical manifold using the blow-up technique. The existence of two primary canards is known provided a nonresonance condition $\mu \notin \mathbb{N}$ is satisfied, where $\mu = \lambda_1/\lambda_2$ denotes the ratio of the eigenvalues of the associated folded singularity of the reduced flow. We show that, due to resonances, bifurcation of secondary canards occurs. We give a detailed geometric explanation of this phenomenon using an extension of Melnikov theory to prove a transcritical bifurcation of canards for odd $\mu$. Furthermore, we show numerically the existence of a pitchfork bifurcation for even $\mu$ and a novel turning point bifurcation close to $\mu \in \mathbb{N}$. We conclude the existence of $[(\mu-1)/2]$ secondary canards away from the resonances. Finally, we apply our results to a network of Hodgkin–Huxley neurons with excitatory synaptic coupling and explain the observed slowing of the firing rate of the synchronized network due to the existence of canards of folded node type.

**Key words.** singular perturbation, canard solution, blow-up, Melnikov theory, invariant manifolds

**AMS subject classifications.** 34E15, 34C30, 34C15, 37N25, 92C20

**DOI.** 10.1137/030601995

## 1. Introduction.

*Canards* were discovered and first analyzed by French mathematicians [BCDD81] who studied relaxation oscillators in $\mathbb{R}^2$, in particular the van der Pol oscillator. There the *canard phenomenon* explains the very fast transition upon variation of a parameter from a small amplitude limit cycle via *canard cycles* to a large amplitude relaxation cycle. This very fast transition called *canard explosion* happens in an exponentially small parameter interval. Thus it is hard to detect and seems to be more like a canard in a (news)paper. Furthermore, the shape of a canard cycle in the phase plane resembles that of a duck (see Figure 1). So the notion "canard" was born and the chase on these creatures began with either nonstandard [BCDD81] or "standard" [Eck83] methods. To be more precise, the main mathematical methods to analyze the canard phenomenon are nonstandard analysis (see, e.g., [BCDD81, Die84]), matched asymptotic expansions (see, e.g., [Eck83, MKKR94]), and the blow-up technique (see, e.g., [DR96, KS01]), which extends geometric singular perturbation theory known as Fenichel theory to nonhyperbolic points.

Canards are a phenomenon occurring in *slow-fast systems*; i.e., they occur in systems of the form

$$\begin{aligned} \dot{u} &= g(u, v, \varepsilon), \\ \varepsilon \dot{v} &= f(u, v, \varepsilon), \end{aligned} \tag{1.1}$$

*Received by the editors November 26, 2003; accepted for publication (in revised form) by T. Kaper August 18, 2004; published electronically February 22, 2005. This research was supported by the National Science Foundation under agreement 0112050.

http://www.siam.org/journals/siads/4-1/60199.html

†Mathematical Biosciences Institute, Ohio State University, 231 West 18th Ave, Columbus, OH 43210 (wm@mbi.osu.edu).

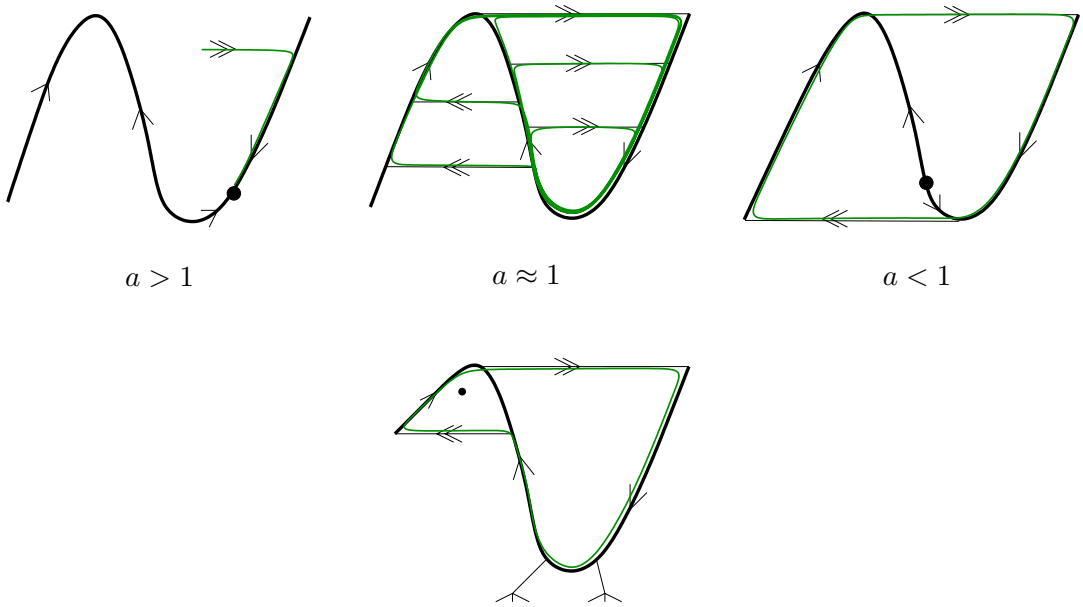


**Figure 1.** *Phase plane (Liénard plane) of the van der Pol relaxation oscillator* $\ddot{z} + \nu(z^2 - 1)\dot{z} + z = a$ *with* $a > 0$ *and* $\nu \gg 1$. *The cubic shaped curve is the critical manifold of the problem, i.e., nullcline of the fast flow (indicated by double arrows). For* $a > 1$ *the system is in an excitable state with a stable fixed point on the attracting right branch of the cubic shaped nullcline. For* $a < 1$, *this equilibrium has moved over the "knee" of the nullcline to the repelling middle branch and the system is in an oscillatory state. The transition happens in an exponentially small parameter interval near* $a = 1$ *through a "canard explosion" where solutions follow the repelling middle branch of the nullcline for a certain amount of time before being repelled forming canard cycles.*

with $u \in \mathbb{R}^n$, $v \in \mathbb{R}^m$, sufficiently smooth functions $g, f$, and small parameter $0 < \varepsilon \ll 1$. Let $\tau$ denote the independent variable of (1.1), which is referred to as the *slow time scale*. By switching to the *fast time scale* $t := \tau/\varepsilon$, one obtains the equivalent system

$$\begin{aligned} u' &= \varepsilon g(u, v, \varepsilon), \\ v' &= f(u, v, \varepsilon). \end{aligned} \tag{1.2}$$

One tries to analyze the dynamics of system (1.1) by suitably combining the dynamics of the *reduced problem*,

$$\begin{aligned} \dot{u} &= g(u, v, 0), \\ 0 &= f(u, v, 0), \end{aligned} \tag{1.3}$$

and the dynamics of the *layer problem*,

$$\begin{aligned} u' &= 0, \\ v' &= f(u, v, 0), \end{aligned} \tag{1.4}$$

which are the limiting problems for $\varepsilon \to 0$ on the slow and the fast time scales, respectively. The phase space of (1.3) is the *critical manifold* $S$ defined by $S := \{(u, v) \in \mathbb{R}^n \times \mathbb{R}^m : f(u, v, 0) = 0\}$. For system (1.4), $S$ corresponds to a set of equilibria. By Fenichel theory [Fen79], normally hyperbolic pieces of $S$ perturb to nearby *slow invariant manifolds* $S_\varepsilon$ of system (1.1) with the flow given approximately by the flow of system (1.3). The most common case where normal hyperbolicity breaks down are folded critical manifolds. Well-known phenomena in this context are relaxation oscillations, i.e., solutions slowly moving toward a fold, jumping from the fold point to another attracting branch of $S$, following the slow dynamics again until another fold point is reached, jumping again, etc., and possibly forming periodic solutions (see Figure 1, $a < 1$). In contrast, canard solutions are solutions which slowly move toward the fold, cross the fold, and surprisingly follow the repelling (middle) branch of $S$ for a certain amount of time before being repelled to another attracting branch of $S$ possibly forming canard cycles (see Figure 1, $a \approx 1$).

In chemical systems, canard explosions have been identified and associated with a dramatic change in the amplitude and period of a periodic solution within a very small range of a control parameter (see, e.g., [BB91, PGS91, Moe02]). Furthermore, canards play an important role in diffusion induced instabilities [BDE95] and spatial localization of oscillation patterns [RKZE03]. In biological systems, the canard phenomenon is often encountered with a delay effect like a delayed onset of firing or bursting in neurons [BCE97]. All these studies on canards have been for two-dimensional (2D) systems, respectively, systems with just one slow variable (we denote these canards as *canards in* $\mathbb{R}^2$). The downside for real experiments is that these canards in $\mathbb{R}^2$ can hardly be detected. First, the parameter interval where canard cycles occur is exponentially small. Second, the delay effect due to canards vanishes under the influence of noise in the experimental system; i.e., noise kicks solutions immediately away from the repelling branch of the critical manifold as soon as they have passed the fold. Thus the only observation usually made is a transition from stable steady state to relaxation oscillations (hard transition).

This situation changes if there is a second slow variable in the system under consideration. Canards in these systems are generic (we denote them *canards in* $\mathbb{R}^3$); i.e., they are insensitive to small parameter changes. There are different types of such canards, and Benoît [Ben83] was the first who studied them by means of nonstandard analysis. Furthermore, canards in $\mathbb{R}^3$ shape the phase space under consideration significantly; e.g., canards in $\mathbb{R}^3$ are separatrices in the phase space, which divide domains with large relaxation oscillations from domains with small amplitude oscillations. Mixed mode oscillations (MMOs) [PPS92], for which the oscillatory cycle consists of a number of large amplitude oscillations and a number of small amplitude oscillations, are often found in chemical systems. It was shown for a three-dimensional (3D) autocatalator model in [MSLG98] that a canard serves as a separatrix and plays a key role in understanding these oscillation patterns. We show in this work that significant delays in firing rates of neurons can be explained by the existence of canards in $\mathbb{R}^3$ and that this behavior is closely related to the phenomenon of MMOs. This canard induced phenomenon is robust under noise; i.e., the delay can be observed experimentally. In general, canards in $\mathbb{R}^3$ are indicators of more complex and chaotic behavior. The van der Pol oscillator with periodic forcing is a prototypical example exhibiting chaotic behavior, which is partly due to the existence of canards in $\mathbb{R}^3$ [BEG03].

We want to emphasize that a second slow variable is needed to unfold canards; i.e., canards are just generic (robust) objects in $\mathbb{R}^3$, while they are degenerate objects in $\mathbb{R}^2$. To restate it from a bio-scientific point of view, "Canards should be studied in vivo, not in vitro."

Canards in $\mathbb{R}^3$ have been classified and analyzed in [SW01] using geometric singular perturbation theory. In the following we recall the classification and refer for details to [SW01]. We consider system (1.1) with slow variables $(x, y) = u \in \mathbb{R}^2$ and fast variable $z = v \in \mathbb{R}$, i.e.,

$$\begin{aligned} \dot{x} &= g_1(x, y, z, \varepsilon), \\ \dot{y} &= g_2(x, y, z, \varepsilon), \\ \varepsilon \dot{z} &= f(x, y, z, \varepsilon). \end{aligned} \tag{1.5}$$

We assume that the critical manifold $S := \{(x, y, z) \in \mathbb{R}^3 : f(x, y, z, 0) = 0\}$ is a nondegenerate folded surface in a neighborhood of the origin. Sufficient conditions for this assumption are

$$\begin{aligned} f(0,0,0,0) &= 0, \qquad & f_z(0,0,0,0) &= 0, \\ f_x(0,0,0,0) &\neq 0, \qquad & f_{zz}(0,0,0,0) &\neq 0, \end{aligned} \tag{1.6}$$

i.e., $S = S_a \cup L \cup S_r$ with attracting branch $S_a := \{(x, y, z) \in S : f_z(x, y, z) < 0\}$, fold-curve $L := \{(x, y, z) \in S : f_z(x, y, z) = 0\}$, and repelling branch $S_r := \{(x, y, z) \in S : f_z(x, y, z) > 0\}$ (see Figure 2). Note that $S$ is locally given as a graph $x = \varphi(y, z)$, and the fold-curve $L$ can be locally parameterized by $y$, i.e., points $p \in L$ are given by $(\xi(y), y, \zeta(y))$, $y \in I$.

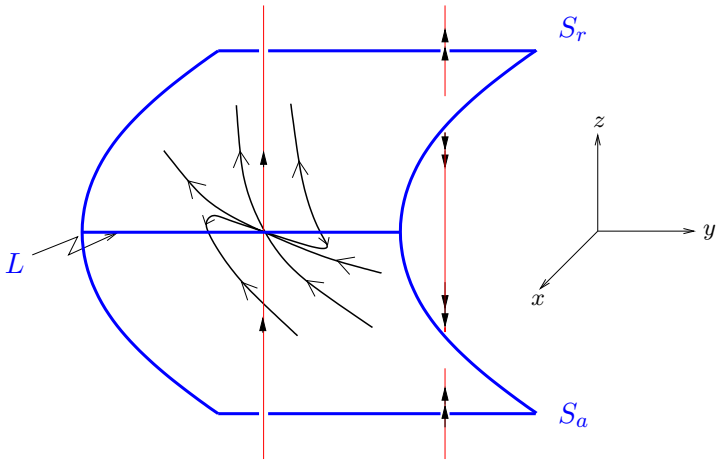


**Figure 2.** *Folded critical manifold $S$ with attracting branch $S_a$, fold-curve $L$, and repelling branch $S_r$. The reduced flow on $S$ is shown in a neighborhood of a folded node singularity.*

Because $S$ is given as a graph $x = \varphi(y, z)$, we project the reduced system onto the $(y, z)$-plane and obtain

$$\begin{pmatrix} 1 & 0 \\ 0 & -f_z \end{pmatrix} \begin{pmatrix} \dot{y} \\ \dot{z} \end{pmatrix} = \begin{pmatrix} g_2 \\ f_x\, g_1 + f_y\, g_2 \end{pmatrix} \Big|_{x=\varphi(y,z)}. \tag{1.7}$$

System (1.7) is singular at the fold-curve $(f_z|_L = 0)$. The standard existence and uniqueness results for differential equations do not hold there. In particular, different solutions of

system (1.7) may approach the same point on the fold-curve in finite forward and backward time. We will see that this allows the existence of solutions of the reduced problem, which pass from the attracting manifold $S_a$ to the repelling manifold $S_r$.

To obtain the dynamics of the reduced problem, we *desingularize* system (1.7) by multiplying the right-hand side of (1.7) by $-f_z$ (rescaling time) and dividing the second equation by this factor, which gives the *desingularized system*

$$\begin{pmatrix} \dot{y} \\ \dot{z} \end{pmatrix} = \begin{pmatrix} -f_z\, g_2 \\ f_x\, g_1 + f_y\, g_2 \end{pmatrix}\Big|_{x=\varphi(y,z)}. \tag{1.8}$$

We set

$$l(y) := (f_x\, g_1 + f_y\, g_2)|_{p\in L}$$

and assume

$$l(0) = 0. \tag{1.9}$$

Because of (1.9) and $f_z(0,0,0,0) = 0$ from (1.6), the desingularized system (1.8) has an equilibrium at the origin. This equilibrium determines the phase portrait in the neighborhood of the origin. We obtain the phase portrait of the reduced system (1.7) by changing the direction of the flow in the phase portrait of the desingularized system (1.8), where $f_z > 0$, i.e., on the repelling branch $S_r$. Note that the singularity at the origin of the reduced system (1.7) is not an equilibrium. Solutions of the desingularized system (1.8), which approach the origin in backward and forward time in a hyperbolic direction, correspond to solutions of the reduced problem (1.7) passing through the origin with nonzero speed, which is due to a cancellation of a simple zero in the second equation of (1.7). Such a solution is called a *singular canard*. In correspondence with the phase portrait of the desingularized system (1.8), the singularity at the origin of the reduced system (1.7) is classified as a *folded saddle*, *folded node*, *folded degenerate node*, or *folded saddle-node (type* I/II*)* (see Figures 3–4).

Let $\lambda_{1/2}$ denote the eigenvalues of the linearization at the origin of (1.8), and let

$$\mu := \frac{\lambda_1}{\lambda_2}. \tag{1.10}$$

A necessary condition to have canards of folded saddle or folded node type, i.e., $\lambda_1 \cdot \lambda_2 \neq 0$, is

$$g_2(0,0,0,0) \neq 0, \tag{1.11}$$

which follows by linearization of system (1.8) at the origin. Note that in the folded node case $\mu > 0$ we have a whole sector of singular canards (shadowed region in Figure 3) corresponding to the weak eigendirection (dashed line in Figure 3) of system (1.8) at the origin. Similarly, a whole sector of singular canards exists in the degenerate folded node case $\mu = 1$. All other singular canards (bold lines in Figures 3 and 4) correspond one-to-one to an eigendirection of (1.8) at the origin.

The goal is to show persistence of singular canards under small perturbations $0 < \varepsilon \ll 1$ for system (1.5). Fenichel theory [Fen79, Jon95] shows that, outside a small neighborhood $U_1$

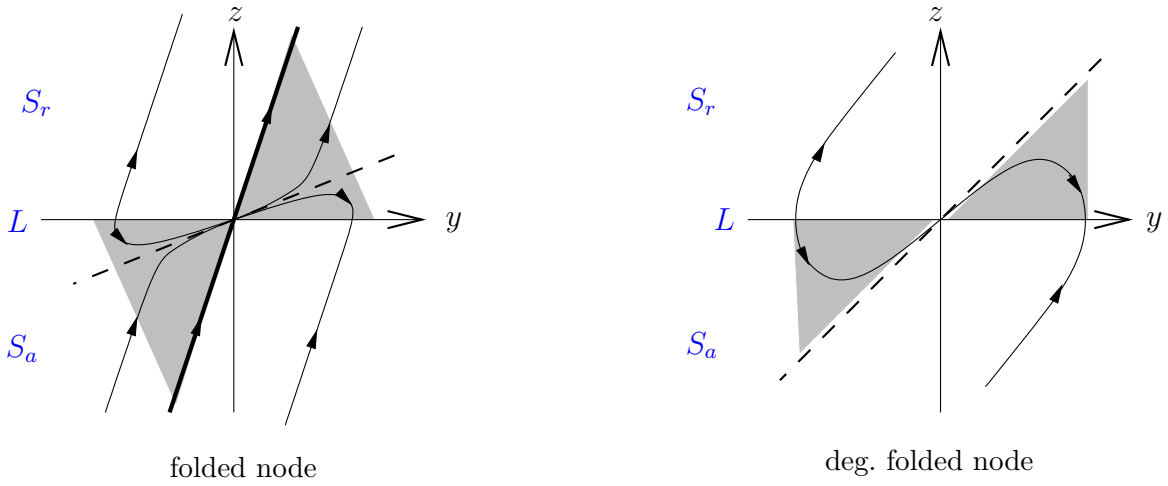


**Figure 3.** *The reduced flow near a folded node singularity projected onto the $(y, z)$ plane. The $y$-axis represents the fold-curve $L$, $z < 0$ corresponds to the attracting manifold $S_a$, and $z > 0$ corresponds to the repelling manifold $S_r$. The shadowed regions show a whole sector of singular canards which cross over to $S_r$ through the folded node singularity at the origin.*

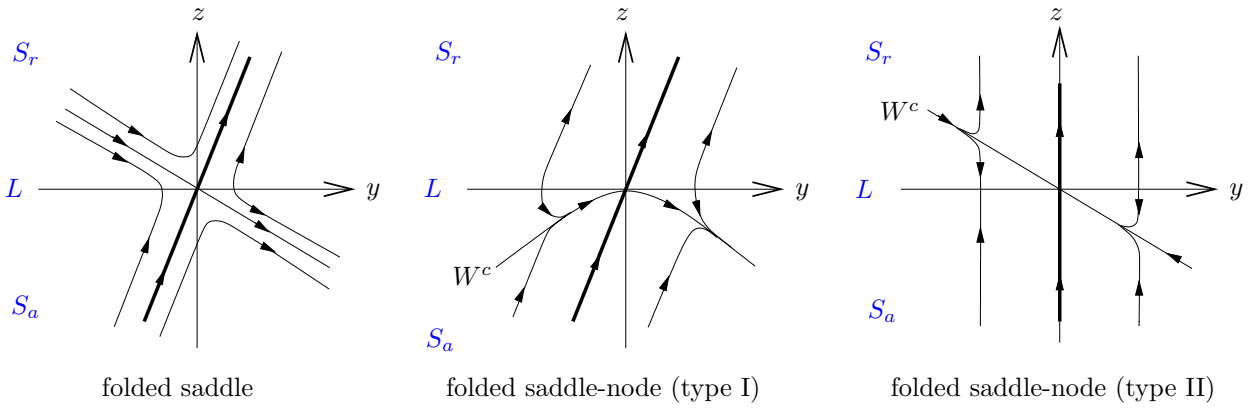


**Figure 4.** *The reduced flow near a folded saddle, respectively, saddle-node singularity, projected onto the $(y, z)$ plane. The $y$-axis is the fold-curve $L$, $z < 0$ corresponds to the attracting manifold $S_a$, and $z > 0$ corresponds to the repelling manifold $S_r$. There exist unique singular canards (bold lines) which cross over to $S_r$ through the folded singularity at the origin.*

of the fold-curve $L$, the manifolds $S_a$ and $S_r$ perturb smoothly to locally invariant manifolds $S_{a,\varepsilon}$ and $S_{r,\varepsilon}$ for sufficiently small $\varepsilon \neq 0$. Clearly, the slow manifolds can be extended in forward and backward time by the flow; however, their behavior is then not controlled by the singular limit problems introduced so far. Using the blow-up method [DR96, KS01], it is possible to study the intersection of these manifolds $S_{a,\varepsilon}$ and $S_{r,\varepsilon}$, which correspond to the existence of a so-called *maximal canard*. Note that any solution which is exponentially close to a maximal canard on $S_{a,\varepsilon}$ is a canard solution; i.e., these solutions follow the maximal canard on the repelling branch $S_{r,\varepsilon}$ for a certain amount of time before they get repelled (either back or away). Thus a maximal canard defines a family of canard solutions.

The pioneering work on canards in $\mathbb{R}^3$ is due to Benoît [Ben83, Ben90, Ben01]. Based on methods from nonstandard analysis, he proved the existence of canard solutions in the folded saddle case. In the folded node case, he showed the existence of a pair of maximal canards provided the nonresonant condition $\mu \notin \mathbb{N}$ is satisfied. Similar results by means of matched asymptotic expansion can be found in Mishchenko et al. [MKKR94]. Szmolyan and Wechselberger [Wec98, SW01] showed by using geometric singular perturbation theory and the blow-up technique that a (unique) singular canard in the folded saddle case and a (unique) singular canard in the folded node case corresponding to the strong eigendirection of system (1.8) always perturbs to a maximal canard solution of system (1.5); i.e., the slow manifolds $S_{a,\varepsilon}$ and $S_{r,\varepsilon}$ intersect transversally. Similarly, a singular canard in the folded saddle-node (type II) case perturbs to a maximal canard.

In this work, we focus on the existence and bifurcation of maximal canards corresponding to the sector of singular canards of folded node type. It was shown in [SW01] that a transverse intersection of $S_{a,\varepsilon}$ and $S_{r,\varepsilon}$ exists corresponding to the weak eigendirection (the sector of singular canards) in the folded node case provided that $\mu$ is *not* a natural number, i.e., the existence of a (primary) maximal canard. If $n-1 < \mu < n$, then the slow manifolds $S_{a,\varepsilon}$ and $S_{r,\varepsilon}$ twist $n-1$ times around the corresponding maximal canard in the neighborhood of the fold curve. In the resonant cases, $\mu \in \mathbb{N}$, transversality is violated, and we show that bifurcations of maximal canards occur. This is the mechanism that creates new *secondary maximal canards* nearby, i.e., other transverse intersections of $S_{a,\varepsilon}$ and $S_{r,\varepsilon}$. The proof of the existence and bifurcation of these secondary canards is the main part of this work and can be viewed as complementary work on the geometric analysis of canards in $\mathbb{R}^3$ started in [SW01, Wec02].

We want to point out that a geometric approach is well suited to study the bifurcation mechanism of secondary canards from a primary canard. Benoît [Ben90, Ben01] mentioned the existence of secondary canards and gave numerical evidence of their existence. Guckenheimer and Haiduc [GH04] showed numerically secondary canards for large resonances $\mu \gg 1$. Their analysis was based on a perturbation of a folded saddle-node ($\mu \to \infty$). They argued by the rotational properties of the invariant manifolds that the number of secondary canards goes to infinity for $\mu \to \infty$ but without focusing on the underlying bifurcation mechanism.

The article is organized as follows. In section 2, we do the analysis and restate results on primary maximal canards in $\mathbb{R}^3$ given in [SW01], which is needed for the analysis of secondary maximal canards. After a preliminary transformation, which brings system (1.5) into a canonical form near a folded node singularity, we give a detailed geometric analysis using the blow-up technique. We are focusing especially on the blown-up reduced flow and its extension onto the blown-up locus, which extends the analysis done in [SW01]. We restate the results on the existence of two primary maximal canards for $\mu \notin \mathbb{N}$ and the rotational properties of the invariant manifolds near the primary (weak) maximal canard corresponding to the sector of singular canards.

In section 3, we focus on the analysis of the resonant cases $\mu \in \mathbb{N}$. We derive bifurcation equations for singular canards by applying an extension of Melnikov theory given in [Wec02]. Assumptions of this theory are naturally fulfilled in the blow-up analysis by the extensions of center-like manifolds $M_a$, respectively, $M_r$, from the entry chart $\kappa_1$ into the classical chart $\kappa_2$ on the blown-up locus. Thus the bifurcation analysis is naturally carried out in the classical

chart $\kappa_2$. We show the existence of a transcritical bifurcation of singular canards for odd $\mu$, which is the main analytical result of this work.

In section 4, we give numerical evidence for the derived transcritical bifurcation for odd $\mu$ and for a pitchfork bifurcation for even $\mu$. Furthermore, we show that one branch of secondary canards of the transcritical bifurcation and the two branches of secondary canards of the pitchfork bifurcation exist just in a very small neighborhood $U$ of $\mu \in \mathbb{N}$. The reason is a folding back mechanism of the invariant manifolds on one side of the primary (weak) singular canard due to turning points of the reduced flow nearby. This causes a "degenerate" bifurcation in the neighborhood $U$ of the transcritical, respectively, pitchfork, bifurcation, and we call this phenomenon a *turning point bifurcation*. Thus the only persistent branch of secondary canards outside $U$ bifurcates from the transcritical bifurcation for $\mu > (2n+1)$, $n \in \mathbb{N}$. We conclude the existence of $[(\mu-1)/2]$ secondary canards for $\mu > 3$ and outside $U$, where $[(\mu-1)/2]$ denotes the greatest integer less than or equal to $(\mu-1)/2$.

In section 5, we apply these results to a network of Hodgkin–Huxley (HH) neurons studied in Drover et al. [DRSE04]. The network synchronizes rapidly under synaptic excitatory coupling and has a low firing rate of about 10 Hz compared to the intrinsic firing rate of an individual neuron of about 100 Hz. Because of synchrony, it suffices to study a single self-coupled HH neuron. Standard reduction procedures reduce the HH model to a simpler one with one slow variable and one fast variable. An extra synaptic variable with slow decay rate completes the reduction of the model studied by Drover et al. [DRSE04]. This reduced HH model has the same qualitative features as a FitzHugh–Nagumo (FHN) model, a cubic shaped critical manifold (V-nullcline) with one equilibrium close to the lower fold on the repelling middle branch; i.e., the uncoupled neuron is in an oscillatory state and fires action potentials (with high frequency). For this reason, we study a self-coupled FHN model and show the existence of canards of folded node type in the silent phase where the synaptic variable is the second slow variable. This fact explains the lowering of the firing rate due to synaptic excitatory coupling as compared to the uncoupled neuron.

## 2. Blow-up analysis.

In this section, we review some of the results from [SW01]. We focus especially on the blow-up of the reduced flow near a folded node (Figure 3) and its extension onto the blown-up sphere. As a starting point for our analysis, we show the following.

Proposition 2.1. *Assume that system* (1.5) *satisfies conditions* (1.6), (1.9) *and that we are in the folded node scenario. Then there exist a smooth change of time and a smooth change of coordinates, which brings system* (1.5) *to the form*

$$\begin{aligned} \dot{x} &= \frac{1}{2}\mu y - (\mu+1)z + O(x,\varepsilon,(y+z)^2), \\ \dot{y} &= 1, \\ \varepsilon\dot{z} &= x + z^2 + O(xz^2, z^3, xyz) + \varepsilon O(x,y,z,\varepsilon), \end{aligned} \tag{2.1}$$

*in a neighborhood of the origin where* $\lambda_1 = -\mu \in \mathbb{R}^-$ *and* $\lambda_2 = -1$ *correspond to the eigenvalues of the linearization of the desingularized flow of* (2.1).

*Proof.* Remember that a necessary condition to have canards of folded node type is $g_2(0,0,0,0) \neq 0$ (1.11). Thus we first change time by $d\bar{\tau} = d\tau\, g_2(x,y,z,\varepsilon)$ in (1.5). As was shown in the proof of Proposition 2.1 in [SW01], we rectify the fold-curve $L$ along the

$y$-axis by a coordinate transformation $(x, y, z) \mapsto (x - \xi(y), y, z - \zeta(y))$. Then a Taylor expansion of the functions $f, g_1$, together with a sequence of linear and near identity transformations (see, e.g., [GH83]), gives

$$\begin{aligned} \dot{x} &= by + cz + O(x, \varepsilon, (y+z)^2), \\ \dot{y} &= 1, \\ \varepsilon \dot{z} &= x + z^2 + O(xz^2, z^3, xyz) + \varepsilon O(x, y, z, \varepsilon), \end{aligned} \tag{2.2}$$

with $(b, c) \in \mathbb{R}^2$ computable constants (we omit new coordinate and function notation). In a last step we transform system (2.2) by

$$(x, y, z, t, \varepsilon) \mapsto (\tilde{\lambda}^2 x, \tilde{\lambda}^2 y, -\tilde{\lambda} z, \tilde{\lambda}^2 t, -\tilde{\lambda}^3 \varepsilon), \tag{2.3}$$

where $\tilde{\lambda}$ satisfies the characteristic equation $\tilde{\lambda}^2 - \tilde{\lambda} c + 2b = 0$ of the linearization of the desingularized system of (2.2). With the definition of the parameter

$$\mu := \frac{\tilde{\lambda}_1 \tilde{\lambda}_2}{\tilde{\lambda}^2}, \tag{2.4}$$

we obtain system (2.1). The corresponding eigenvalues of the linearization of the desingularized system of (2.1) are $\lambda_1 = -\mu$ and $\lambda_2 = -1$. Thus the notion of the eigenvalue $\lambda_1 = -\mu$ becomes clear by definition (1.10) of the resonant parameter. ■

*Remark.* For $\mu \in [1, \infty)$, $\lambda_1 = -\mu$, and $\lambda_2 = -1$, all resonances of (1.10) are realized, and $\lambda_2 = -1$ corresponds to the sector of singular canards. We are focusing on this scenario. Of course the same can be realized for $\mu \in (0, 1]$, $\lambda_1 = -1$, and $\lambda_2 = -\mu$, where again $\lambda_2$ corresponds to the sector of singular canards.

The critical manifold $S$ of (2.1) is approximately a parabolic cylinder near the origin where the lower branch $S_a$ is attracting while the upper branch $S_r$ is repelling for the corresponding layer problem (see Figure 2). The layer problem is the one-dimensional system obtained by changing to the fast time scale $t = \tau/\varepsilon$ in (2.1) and taking the limit $\varepsilon \to 0$. The fast fibers are simply lines in the $z$ direction.

Fenichel theory [Fen79, Jon95] shows that outside a small neighborhood $U_1$ of the fold-curve $L$ the manifolds $S_a$ and $S_r$ perturb smoothly to locally invariant manifolds $S_{a,\varepsilon}$ and $S_{r,\varepsilon}$ for sufficiently small $\varepsilon \neq 0$. Moreover, there exist smooth invariant foliations of the manifold $W^s(S_{a,\varepsilon}) \cap V_1$ in a neighborhood $V_1$ of the base $S_{a,\varepsilon}$ and smooth invariant foliations of the manifold $W^u(S_{r,\varepsilon}) \cap V_2$ in a neighborhood $V_2$ of the base $S_{r,\varepsilon}$.

Note that the slow manifolds are obtained as sections $\varepsilon = \text{const}$ of 3D, locally invariant, center-like manifolds $M_a$, respectively, $M_r$, of the extended (fast) system

$$\begin{aligned} x' &= \varepsilon \left( \frac{1}{2} \mu y - (\mu + 1) z + O(x, \varepsilon, (y+z)^2) \right), \\ y' &= \varepsilon, \\ z' &= x + z^2 + O(xz^2, z^3, xyz) + \varepsilon O(x, y, z, \varepsilon), \\ \varepsilon' &= 0 \end{aligned} \tag{2.5}$$

in the extended phase-space $\mathbb{R}^4$. For the extended system $S \times \{0\}$ is a manifold of equilibria. Outside of a neighborhood $U_1$ of the fold-curve $L$, the linearization of (2.5) at points $S_a \times \{0\}$ has a triple zero eigenvalue and one negative eigenvalue uniformly bounded away from zero. This allows us to prove the existence of the attracting center-like manifold $M_a$. The repelling center-like manifold $M_r$ is obtained in a similar way. At the fold-curve the linearization has a quadruple zero eigenvalue, and the construction of the slow manifolds breaks down. Clearly, the slow manifolds can be extended in forward and backward time by the flow; however, their behavior is then not controlled by the singular limit problems introduced so far.

For that purpose, we are using the *blow-up* technique (see, e.g., [DR96], [KS01]) to desingularize the flow near nilpotent equilibria like the points on the fold-curve. The blow-up technique is a coordinate transformation by which the degenerate equilibrium at the origin of system (2.5) is blown up to a sphere $S^3$. With this procedure, one gains enough hyperbolicity to apply standard tools of dynamical systems theory. Figure 5 shows the blow-up for fixed $y = 0$.

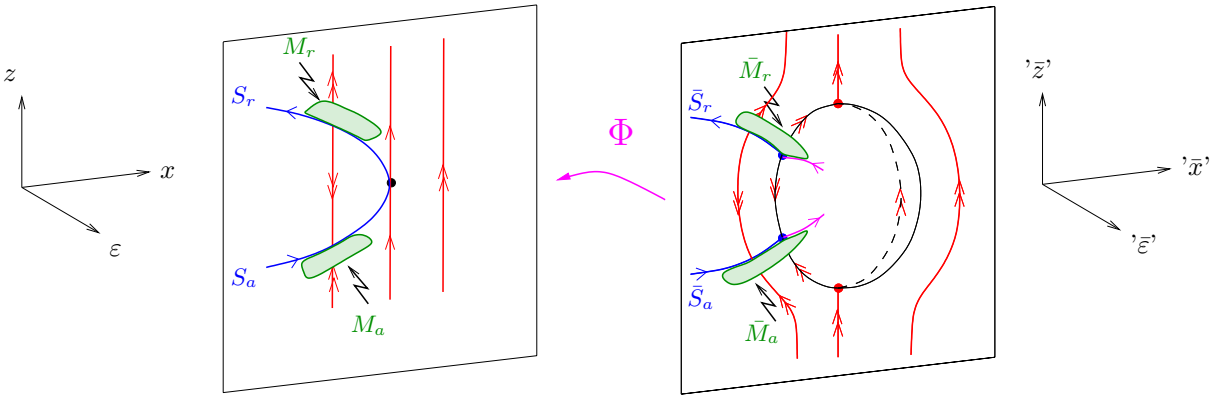


**Figure 5.** *The blow-up transformation $\Phi$ projected onto $y = 0$: The folded singularity (black dot) is blown up to a sphere $S^3$. Due to the blow-up, we gain an extra hyperbolic direction at the equator of the sphere (the fast flow is indicated by double red arrows) which allows the extension of the center-like manifolds $M_a$ and $M_r$ obtained by Fenichel theory (away from the fold) onto the blown-up sphere.*

In our case, the blow-up transformation $\Phi : B = S^3 \times \mathbb{R} \to \mathbb{R}^4$ is given by

$$x = r^2\bar{x},\ y = r\bar{y},\ z = r\bar{z},\ \varepsilon = r^2\bar{\varepsilon}, \tag{2.6}$$

with $(\bar{x}, \bar{y}, \bar{z}, \bar{\varepsilon}) \in S^3$. An exposition of the blow-up technique suitable for the analysis of singularly perturbed systems can be found in [SW01]. For the analysis of system (2.5), it suffices to consider two charts $\kappa_1$ and $\kappa_2$ defined by $\bar{x} = -1$, respectively, $\bar{\varepsilon} = 1$ (see Figure 6). The singular chart $\kappa_1$ gives the extension of the center-like manifolds $M_a$ and $M_r$ onto the blown-up locus. These manifolds are connected on the blown-up locus by special solutions found in the classical chart $\kappa_2$. These special solutions can be viewed as extensions of singular canards under consideration.

*Remark on notation.* $\bar{P}$ denotes an object in the blow-up which corresponds to an object $P$ in the original problem. If $\bar{P}$ is described in chart $\kappa_i$, then $P_i$ denotes that object in this chart.

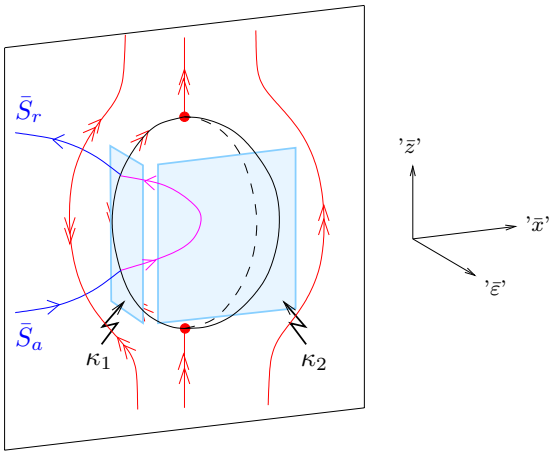


**Figure 6.** *The charts $\kappa_1$ and $\kappa_2$ needed to analyze the blow-up. The singular chart $\kappa_1$ covers the incoming flow and outgoing flow on the blown-up sphere, while the rescaling chart $\kappa_2$ covers the flow on the blown-up sphere.*

**2.1. Dynamics in chart $\kappa_1$.** The blow-up $\Phi_1 : \mathbb{R}^4 \to \mathbb{R}^4$ is obtained by setting $\bar{x} = -1$ in (2.6), i.e.,

$$\Phi_1(r_1, y_1, z_1, \varepsilon_1) = (-r_1^2, r_1 y_1, r_1 z_1, r_1^2 \varepsilon_1).$$

After the transformation of system (2.5) and desingularization, i.e., rescaling time by the factor $r_1$, we obtain

$$\begin{aligned} r_1' &= -\frac{1}{2} r_1 \varepsilon_1 g_{11}(r_1, y_1, z_1, \varepsilon_1), \\ y_1' &= \varepsilon_1 \left(1 + \frac{1}{2} y_1 g_{11}(r_1, y_1, z_1, \varepsilon_1)\right), \\ z_1' &= -1 + z_1^2 + r_1(\alpha_1 z_1^3 + O(r_1)) + \frac{1}{2} \varepsilon_1 z_1 g_{11}(r_1, y_1, z_1, \varepsilon_1), \\ \varepsilon_1' &= \varepsilon_1^2 g_{11}(r_1, y_1, z_1, \varepsilon_1), \end{aligned} \tag{2.7}$$

with

$$g_{11}(r_1, y_1, z_1, \varepsilon_1) = \frac{1}{2}\mu y_1 - (\mu + 1) z_1 + O(r_1).$$

*Remark.* The equations for $r_1'$ and $\varepsilon_1'$ are obtained from $\varepsilon' = 0$, which implies the relation $2 r_1 r_1' \varepsilon_1 + r_1^2 \varepsilon_1' = 0$. Hence, $\varepsilon = r_1^2 \varepsilon_1$ is a constant of motion in chart $\kappa_1$ and the trivial foliation $\varepsilon = \text{const}$ becomes a nontrivial foliation $r_1^2 \varepsilon_1 = \text{const}$ in chart $\kappa_1$.

There exist two invariant subspaces in system (2.7), namely, the hyperplanes $r_1 = 0$ and $\varepsilon_1 = 0$. In their intersection, we find two lines of equilibria $L_{a,1} = (0, y_1, -1, 0)$ and $L_{r,1} = (0, y_1, 1, 0)$ which are normally hyperbolic; the nonzero eigenvalue is $-2$ for $L_{a,1}$ and 2 for $L_{r,1}$.

Furthermore, system (2.7) has in $\varepsilon_1 = 0$ a normally hyperbolic surface $S_{a,1}$ of equilibria emanating from $L_{a,1}$ and a surface $S_{r,1}$ of equilibria emanating from $L_{r,1}$ (see Figure 7). Note

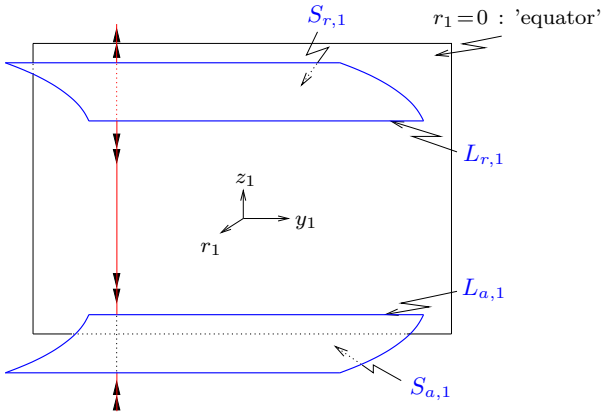


**Figure 7.** *Blown-up attracting and repelling manifolds $S_{a,1}$ and $S_{r,1}$ in hyperplane $\varepsilon_1 = 0$. The normal hyperbolicity of these manifolds is extended to the "equator" of the blown-up sphere; i.e., points on $L_{a,1}$ and $L_{r,1}$ have a nonzero eigenvalue.*

that $S_{a,1}$, respectively, $S_{r,1}$, corresponds to the attracting, respectively, repelling, branch $S_a$, respectively, $S_r$, of the critical manifold. We have gained normal hyperbolicity at the lines $L_{a,1}$ and $L_{r,1}$ due to the blow-up.

In the invariant hyperplane $r_1 = 0$, we recover the lines of equilibria $L_{a,1}$ and $L_{r,1}$ and one additional zero eigenvalue due to the third equation. Hence, there exists a 2D center manifold $C_{a,1}$, respectively, $C_{r,1}$, of the line $L_{a,1}$, respectively, $L_{r,1}$. This center manifold $C_{a,1}$, respectively, $C_{r,1}$, can be viewed as the extension of $S_{a,1}$, respectively, $S_{r,1}$, on the blown-up locus. Furthermore, there is a time reversing symmetry

$$\sigma_1(\varepsilon_1, y_1, z_1, t_1) = (\varepsilon_1, -y_1, -z_1, -t_1) \tag{2.8}$$

of system (2.7) in $r_1 = 0$.

Proposition 2.2 (see [SW01]). *The following hold for system (2.7):*

1. *There exists an attracting 3D center manifold $M_{a,1}$ of the line of equilibria $L_{a,1}$ containing the surface of equilibria $S_{a,1}$ and the center manifold $C_{a,1}$. The branch of $C_{a,1}$ in $r_1 = 0$, $\varepsilon_1 \geq 0$ is unique for $y_1 > -2(\mu+1)/\mu$.*
2. *There exists a repelling 3D center manifold $M_{r,1}$ of the line of equilibria $L_{r,1}$ containing the surface of equilibria $S_{r,1}$ and the center manifold $C_{r,1}$. The branch of $C_{r,1}$ in $r_1 = 0$, $\varepsilon_1 \geq 0$ is unique for $y_1 < 2(\mu+1)/\mu$.*

Note that system (2.7) corresponds to the blow-up of the fast problem (2.5). To obtain the corresponding slow flow on the center manifolds $M_{a,1}$, respectively, $M_{r,1}$, given by

$$z_1(r_1, y_1, \varepsilon_1) = \mp 1 + O(r_1, \varepsilon_1), \tag{2.9}$$

we plug (2.9) into system (2.7) and desingularize, i.e., rescale time by the factor $\varepsilon_1$:

$$\begin{aligned} r_1' &= -\frac{1}{2} r_1 g_{11}(r_1, y_1, z_1(r_1, y_1, \varepsilon_1), \varepsilon_1), \\ y_1' &= 1 + \frac{1}{2} y_1 g_{11}(r_1, y_1, z_1(r_1, y_1, \varepsilon_1), \varepsilon_1), \\ \varepsilon_1' &= \varepsilon_1 g_{11}(r_1, y_1, z_1(r_1, y_1, \varepsilon_1), \varepsilon_1). \end{aligned} \tag{2.10}$$

This system still has $\varepsilon_1 = 0$ and $r_1 = 0$ as invariant hyperplanes. The dynamics in $\varepsilon_1 = 0$ represent the (blown-up) reduced flow on $S_{a,1}$, respectively, $S_{r,1}$, while the dynamics in $r_1 = 0$ represent the extended flow on $C_{a,1}$, respectively, $C_{r,1}$ (on the blown-up sphere).

Lemma 2.1. *The blown-up slow flow given by system (2.10) on the center manifold $M_{a,1}$, respectively, $M_{r,1}$ (2.9), possesses two equilibria $P^-_{\lambda_i}$, $i = 1, 2$, respectively, $P^+_{\lambda_i}$, $i = 1, 2$, on $L_{a,1}$, respectively, $L_{r,1}$, given by*

$$P^{\pm}_{\lambda_i} = \left(0, \pm\frac{2}{|\lambda_i|}, \pm 1, 0\right) = (r_1, y_1, z_1(r_1, y_1, \varepsilon_1), \varepsilon_1), \quad i = 1, 2. \tag{2.11}$$

*For $\mu > 1$, these equilibria are saddles. For $\mu = 1$, these equilibria merge and become a saddle-node.*

Note that in the invariant hyperplane $\varepsilon_1 = 0$ the equilibrium $P^{\pm}_{\lambda_1}$ is a saddle and $P^{\pm}_{\lambda_2}$ is a node. Thus the (unique) strong eigendirection of the folded node corresponds to the (unique) stable, respectively, unstable, manifold of the saddle $P^-_{\lambda_1}$, respectively, $P^+_{\lambda_1}$. The blow-up separates the strong from the weak eigendirection of the folded node. The projection of the reduced flow on $S_{a,1}$ onto the $(y_1, r_1)$-plane is shown in Figure 8.

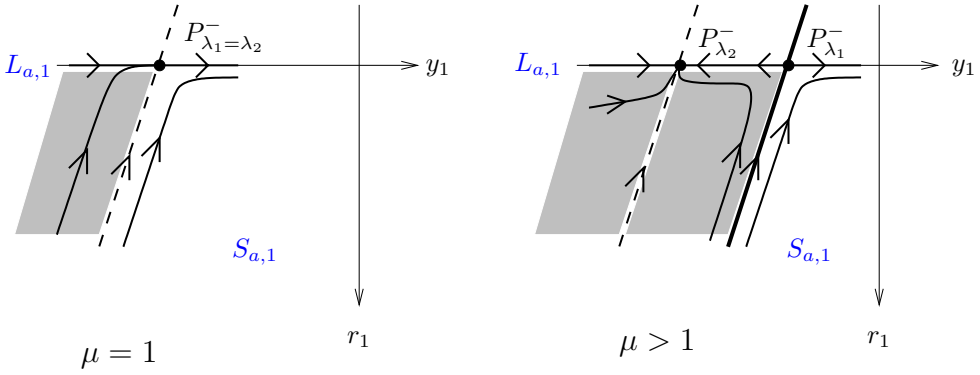


**Figure 8.** *Reduced dynamics on $S_{a,1}$ for $\mu \geq 1$: This shows the blown-up reduced flow near a folded node (Figure 3 for $z \leq 0$). Note that for $\mu > 1$ the strong eigendirection of the folded node splits from the weak eigendirection due to the existence of two equilibria on $L_{a,1}$. Thus the sector of singular canards becomes detached from the unique singular canard corresponding to the strong eigendirection due to the blow-up.*

In the invariant hyperplane $r_1 = 0$, the equilibrium $P^{\pm}_{\lambda_1}$ is a node and $P^{\pm}_{\lambda_2}$ is a saddle. The projection of the extended flow on $C_{a,1}$ onto the $(y_1, \varepsilon_1)$-plane is illustrated in Figure 9. The dotted line in this figure indicates the $\varepsilon_1$-nullcline given by

$$(y_1, \varepsilon_1) = (-2(\mu + 1)/\mu, \varepsilon_1). \tag{2.12}$$

The flow with respect to $\varepsilon_1$ is increasing for $y_1 > -2(\mu+1)/\mu$, i.e., in a neighborhood including the equilibria $P^{\pm}_{\lambda_1}$ and $P^{\pm}_{\lambda_2}$.

Thus the center manifolds $M_{a,1}$ and $M_{r,1}$ can be extended by the flow onto the blown-up locus near these equilibria. The dynamics on the blown-up locus are covered by the classical chart $\kappa_2$. Figure 10 summarizes the invariant dynamics on the center manifold $M_{a,1}$.

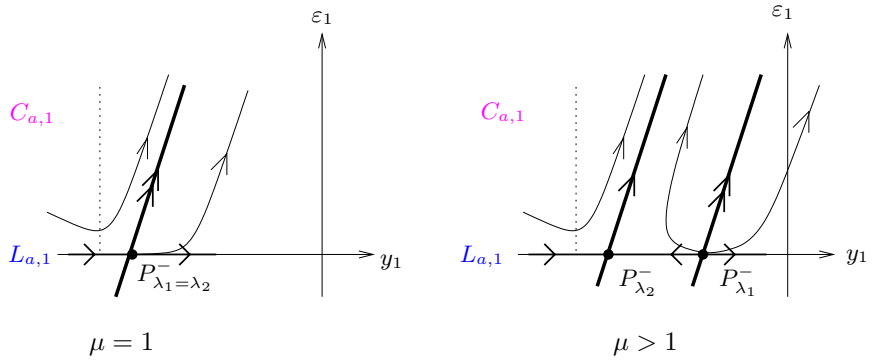


**Figure 9.** *Dynamics on $C_{a,1}$ for $\mu \geq 1$: This shows the extension of the reduced dynamics (Figure 8) onto the blown-up sphere. The dotted line corresponds to the $\varepsilon_1$-nullcline.*

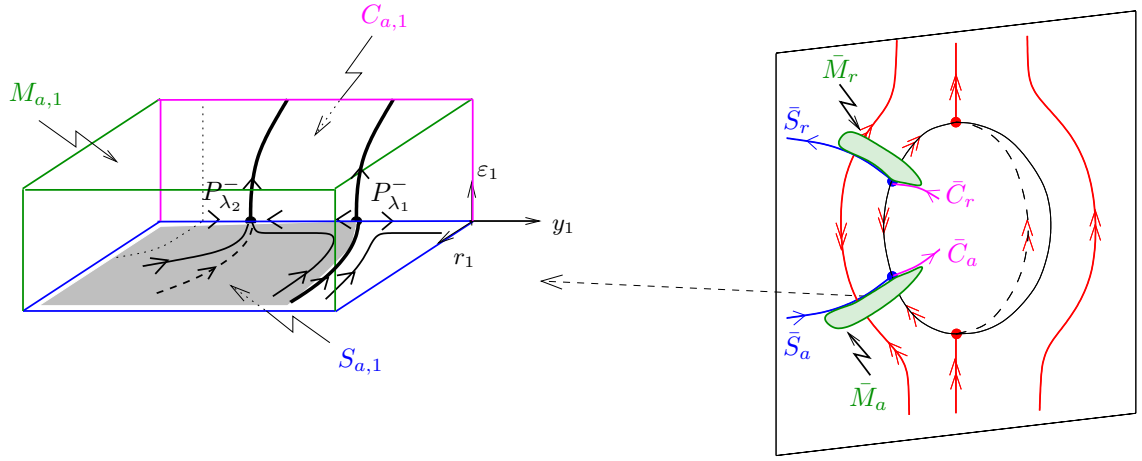


**Figure 10.** *The invariant dynamics on $S_{a,1}$ and $C_{a,1}$ within the 3D center manifold $M_{a,1}$ are shown as well as the corresponding manifolds in the blow-up for $\bar{y} = \text{const}$.*

**2.2. Dynamics in the classical chart $\kappa_2$.** The blow-up $\Phi_2 : \mathbb{R}^4 \to \mathbb{R}^4$ in chart $\kappa_2$ is given by setting $\bar{\varepsilon} = 1$ in (2.6), i.e.,

$$\Phi_2(x_2, y_2, z_2, r_2) = (r_2^2 x_2, r_2 y_2, r_2 z_2, r_2^2).$$

This transformation is just an $\varepsilon$-dependent rescaling of $(x, y, z)$ since $r_2 = \sqrt{\varepsilon}$. After the transformation of system (2.5) and the desingularization (rescaling time by the factor $r_2$) of the blown-up vector field, we obtain

$$\begin{aligned} x_2' &= \frac{1}{2}\mu y_2 - (\mu + 1) z_2 + O(r_2), \\ y_2' &= 1, \\ z_2' &= x_2 + z_2^2 + O(r_2). \end{aligned} \tag{2.13}$$

Setting $r_2 = 0$ gives the unperturbed problem. Two explicit algebraic solutions $\gamma_i$, $i = 1, 2$, are known for the unperturbed problem,

$$\gamma_1(t) = \left(-\frac{\mu^2}{4}t^2 + \frac{\mu}{2}, t, \frac{\mu}{2}t\right), \tag{2.14}$$

$$\gamma_2(t) = \left(-\frac{1}{4}t^2 + \frac{1}{2}, t, \frac{1}{2}t\right), \tag{2.15}$$

where $\gamma_1$, respectively, $\gamma_2$, corresponds to the eigenvalue $\lambda_1 = -\mu$, respectively, $\lambda_2 = -1$, of the linearization of the desingularized flow. Let $\kappa_{12}$ denote the change of coordinates from chart $\kappa_2$ to chart $\kappa_1$ given by

$$\kappa_{12}(x_2, y_2, z_2, r_2) = \left(r_2\sqrt{-x_2}, \frac{y_2}{\sqrt{-x_2}}, \frac{z_2}{\sqrt{-x_2}}, \frac{1}{-x_2}\right), \qquad x_2 < 0. \tag{2.16}$$

We obtain as limiting behavior of the special solutions (2.15) in chart $\kappa_1$

$$\lim_{t\to\pm\infty} \kappa_{12}(\gamma_i(t)) = P^{\pm}_{\lambda_i}, \quad i = 1, 2, \tag{2.17}$$

where $P^{\pm}_{\lambda_i}$ is given by (2.11). The importance of the special solutions $\gamma_i$, $i = 1, 2$, is that they connect the attracting manifold $\bar{M}_a$ across the "upper half" $\bar{\varepsilon} > 0$ of $S^3$ to the repelling slow manifold $\bar{M}_r$. Thus these special solutions are viewed as extensions of the singular canards in $S_{a,1}$ and $S_{r,1}$.

Note that the invariant manifolds $M_{a,1}$ and $M_{r,1}$ transformed into chart $\kappa_2$ describe invariant manifolds $M_{a,2}$ and $M_{r,2}$ of the special solutions $\gamma_i$, $i = 1, 2$, near infinity. These manifolds can be extended by the flow of system $\{(2.13), r_2' = 0\}$. The main property of these invariant manifolds in chart $\kappa_2$ is that solutions within these manifolds are of at most algebraic growth for either $t \to -\infty$ or $t \to \infty$ which is inherited from the properties of these manifolds in chart $\kappa_1$. We summarize the properties of the extended system $\{(2.13), r_2' = 0\}$.

Lemma 2.2. *There exist smooth invariant manifolds $M_{a,2}$ and $M_{r,2}$ intersecting along $\gamma_i$, $i = 1, 2$. $M_{r,2}$ denotes the set of all solutions of system $\{(2.13), r_2' = 0\}$ near $\gamma_i$, $i = 1, 2$, which are of at most algebraic growth for $t \to \infty$. $M_{a,2}$ denotes the set of all solutions of system $\{(2.13), r_2' = 0\}$ near $\gamma_i$, $i = 1, 2$, which are of at most algebraic growth for $t \to -\infty$.*

Note that the 3D manifolds $M_{a,2}$ and $M_{r,2}$ are foliated by the parameter $r_2$ in the extended system $\{(2.13), r_2' = 0\}$. We do our analysis in system (2.13) and denote the 2D invariant manifolds of system (2.13) by $M_{a,2}(r_2)$ and $M_{r,2}(r_2)$, keeping in mind that they represent foliations of the extended invariant manifolds $M_{a,2}$ and $M_{r,2}$. For $r_2 = 0$, we have $M_{a,2}(0) = C_{a,2}$ and $M_{r,2}(0) = C_{r,2}$ which are the extensions of the invariant manifolds $C_{a,1}$ and $C_{r,1}$ of Proposition 2.2 in chart $\kappa_2$.

Furthermore, we denote by $C_{a,2}(\gamma_i)$, respectively, $C_{r,2}(\gamma_i)$, $i = 1, 2$, the invariant manifold $C_{a,2}$, respectively, $C_{r,2}$, locally near one of the special solutions $\gamma_i$, $i = 1, 2$. Studying the intersection of $C_{a,2}(\gamma_1)$ and $C_{r,2}(\gamma_1)$ proves the following proposition.

Proposition 2.3 (see [SW01]). *The slow manifolds $S_{a,\varepsilon}$ and $S_{r,\varepsilon}$ of system (2.1) intersect transversally along a maximal canard corresponding to the strong eigendirection of the folded node for $0 < \varepsilon \ll 1$ and for all $\mu > 1$.*

In the following, we focus on the intersection of $C_{a,2}(\gamma_2)$ and $C_{r,2}(\gamma_2)$ corresponding to the weak eigendirection of the folded node. The goal is to describe all possible solutions of (2.13) near $\gamma_2$ which are of at most algebraic growth for $t \to \pm\infty$. To get a better geometrical understanding for our analysis, we first rectify $\gamma_2$ along the $z_2$-axis. This is done by a coordinate transformation $(x_2, y_2, z_2) \mapsto (x_2 + z_2^2 - 1/2, y_2 - 2z_2, 2z_2)$ which brings system (2.13) to

$$\begin{aligned} x_2' &= \frac{1}{2}\mu y_2 + x_2 z_2 + O(r_2), \\ y_2' &= -2x_2 + O(r_2), \\ z_2' &= 2x_2 + 1 + O(r_2), \end{aligned} \tag{2.18}$$

where we have omitted new coordinate notations. The parameter $\mu$ is the same as in system (2.13). The special solution $\gamma_2$ is transformed to

$$\gamma_2(t) = (0, 0, t), \ t \in \mathbb{R}. \tag{2.19}$$

Let $\hat{x} = (x_2, y_2, z_2)$. We substitute $\hat{x} = \gamma_2(t) + v$, which transforms system (2.18) to the nonautonomous system

$$v' = A(t, \mu_0)v + g(t, v, \mu, r_2), \tag{2.20}$$

with $v = (v_1, v_2, v_3)$, linear part

$$A(t, \mu_0) = \begin{pmatrix} t & \frac{1}{2}\mu_0 & 0 \\ -2 & 0 & 0 \\ 2 & 0 & 0 \end{pmatrix}, \tag{2.21}$$

and

$$g(t, v, \mu, r_2) = f(\gamma(t) + v, \mu, r_2) - f(\gamma(t), \mu_0, 0) - A(t, \mu_0)v, \tag{2.22}$$

where $f$ denotes the right-hand side of (2.18). Furthermore, we denote by $\Phi(t, s)$, $t, s \in \mathbb{R}$, the transition matrix of the variational equation along $\gamma_2$:

$$v' = A(t, \mu_0)v. \tag{2.23}$$

The variational equation can be written as a second order homogeneous equation,

$$v_1'' - tv_1' + (\mu_0 - 1)v_1 = 0, \tag{2.24}$$

which is called the *Weber equation*. If $\mu_0 \in \mathbb{N}$, then the *Hermite polynomial* $H_{\mu_0 - 1}(t/\sqrt{2})$ is a solution of (2.24) of algebraic growth. If $\mu_0 \notin \mathbb{N}$, then all solutions of (2.24) grow exponentially in either forward time or backward time. Thus $\mu_0 \notin \mathbb{N}$ is a sufficient condition to prove transversal intersection of the invariant manifolds $C_{a,2}(\gamma_2)$ and $C_{r,2}(\gamma_2)$ in $r_2 = 0$.

Proposition 2.4 (see [SW01]). *Given system (2.1) and $1 < \mu \notin \mathbb{N}$, the slow manifolds $S_{a,\varepsilon}$ and $S_{r,\varepsilon}$ intersect transversally along a (primary) maximal canard for $0 < \varepsilon \ll 1$ corresponding to the sector of singular canards.*

We introduce an affine coordinate $w = v_1/v_2$ in the variational equation (2.23). This coordinate measures the rotation (in the projective space) of the tangent bundles of $C_{a,2}(\gamma_2)$ and $C_{r,2}(\gamma_2)$ along $\dot{\gamma}_2$ and gives a Riccati equation

$$w' - 2w^2 - tw - \mu_0/2 = 0. \tag{2.25}$$

With the substitution $w = -u'/2u$, this Riccati equation is transformed into a second order linear equation, and we obtain again a Weber equation,

$$u'' - tu' + \mu_0 u = 0. \tag{2.26}$$

Proposition 2.5 (see [SW01]). *Given system* (2.1) *and* $n - 1 < \mu < n$, *the invariant manifolds* $S_{a,\varepsilon}$ *and* $S_{r,\varepsilon}$ *twist* $(n - 1/2)$ *times around the (primary) maximal canard of Proposition* 2.4, *where a twist corresponds to a rotation of* 180°.

At a resonance $\mu_0 \in \mathbb{N}$, the tangent bundles match up, forming a single band with $n$ twists. In these resonant cases $\mu_0 \in \mathbb{N}$, we have a 2D contact of the invariant manifolds $C_{a,2}(\gamma_2)$ and $C_{r,2}(\gamma_2)$, and bifurcation of secondary canards is expected. We will apply an extension of Melnikov theory for invariant manifolds on noncompact domains developed in [Wec02] to analyze these resonances.

**3. Melnikov analysis.** In the global analysis of nonlinear differential equations, the existence and bifurcation of homoclinic/heteroclinic orbits play a central role. One of the analytical methods of dealing with this problem was first introduced by Melnikov [Mel63]. The main idea behind the method is to measure the distance $D$ of the invariant manifolds along a known homoclinic/heteroclinic orbit. The bifurcation equation $D = 0$ then defines homoclinic/heteroclinic connections of the underlying problem under variation of parameters. In general, the bifurcation equation $D = 0$ cannot be solved explicitly. Thus one tries to approximate the distance function $D$ locally near the known homoclinic/heteroclinic orbit. The coefficients in the Taylor expansion of $D$ are called *Melnikov functions* due to his pioneering work.

Usually, Melnikov analysis is carried out under the hypothesis of hyperbolicity of critical points. In [Wec02] this theory was extended to the case of nonhyperbolic critical points that are located at infinity. This is exactly the situation we have in chart $\kappa_2$ where the special solutions $\gamma_i$, $i = 1, 2$, are heteroclinic orbits connecting nonhyperbolic critical points at infinity; i.e., the special solutions represent heteroclinic orbits over the blown-up sphere $S^3$ connecting nonhyperbolic equilibria at the equator of $S^3$ (as shown in Figure 6).

Remember that solutions in $M_{r,2}$, respectively, $M_{a,2}$, are characterized by algebraic growth in forward, respectively, backward, time (Lemma 2.2). All other solutions, which are not in $M_{r,2}$, respectively, $M_{a,2}$, are characterized by exponential growth in forward, respectively, backward, time. We use weaker dichotomy properties of solutions than in the classical approach to derive the bifurcation equation $D = 0$. Note that solutions of $D = 0$ correspond to canard solutions which are of at most algebraic growth in forward and backward time in chart $\kappa_2$.

In the following, we define all objects needed for the derivation of the distance function $D$ between the invariant manifolds $M_{r,2}(r_2)$ and $M_{a,2}(r_2)$ of system (2.20) which are needed

for the bifurcation analysis of canards near $\gamma_2$. For details of the derivation of the distance function $D$, we refer to [Wec02].

The variational equation (2.23) along $\gamma_2$ possesses dichotomy properties; i.e., there exist continuous projection maps $P_+$, respectively, $Q_-$, such that

$$\begin{aligned}\mathcal{R}(P_+(t)) &= T_{\gamma_2(t)}C_{r,2}(\gamma_2), \qquad t \geq 0,\\ \mathcal{R}(Q_-(t)) &= T_{\gamma_2(t)}C_{a,2}(\gamma_2), \qquad t \leq 0.\end{aligned}$$

Hence, we call $\mathcal{R}(P_+(t))$ the center subspace of (2.23) at $t \geq 0$ and $\mathcal{R}(Q_-(t))$ the center subspace of (2.23) at $t \leq 0$. Let the phase-space $\mathbb{R}^3$ split as follows:

$$\mathbb{R}^3 = span\{\dot\gamma_2(0)\} \oplus U \oplus \mathcal{W}, \tag{3.1}$$

with $\|\dot\gamma_2(0)\| = 1$, where

$$\begin{aligned}span\{\dot\gamma_2(0)\} \oplus U &= T_{\gamma_2(0)}C_{r,2}(\gamma_2) \cap T_{\gamma_2(0)}C_{a,2}(\gamma_2),\\ \mathcal{W} &= (T_{\gamma_2(0)}C_{r,2}(\gamma_2) + T_{\gamma_2(0)}C_{a,2}(\gamma_2))^\perp.\end{aligned}$$

Note that $\mathcal{W}$ denotes the subspace of all bounded solutions which decays exponentially in forward and backward time of the adjoint equation of (2.23) given by

$$\psi' + A(t,\mu_0)^T\psi = 0. \tag{3.2}$$

Next we define Banach spaces suitable for our problem,

$$C_b^0(\mathbb{R}_+,\mathbb{R}^3) := \Big\{v \in C^0(\mathbb{R}_+,\mathbb{R}^3) \;\Big|\; \|v\|_+ := \sup_{t\geq 0}\{\|v(t)\|\cdot t^{-\delta}\} < \infty\Big\}, \tag{3.3}$$

$$C_b^0(\mathbb{R}_-,\mathbb{R}^3) := \Big\{v \in C^0(\mathbb{R}_-,\mathbb{R}^3) \;\Big|\; \|v\|_- := \sup_{t\leq 0}\{\|v(t)\|\cdot |t|^{-\delta}\} < \infty\Big\}, \tag{3.4}$$

with fixed $\delta \in \mathbb{N}$ sufficiently large. Thus solutions of (2.20) which are in these Banach spaces determine the 2D invariant manifolds $M_{r,2}(r_2)$, respectively, $M_{a,2}(r_2)$. Using the variation of constant formula for solutions of (2.20), it follows that $v \in C_b^0(\mathbb{R}_+,\mathbb{R}^3)$, respectively, $v \in C_b^0(\mathbb{R}_-,\mathbb{R}^3)$, is a solution of (2.20) if and only if there exists a vector $\xi \in \mathcal{R}(P_+(0)) = \mathcal{R}(Q_-(0))$ such that

$$v_+(t) = \Phi(t,0)\xi + \int_0^t \Phi(t,s)P_+(s)g(s,v_+,\mu,r_2)\,ds + \int_\infty^t \Phi(t,s)Q_+(s)g(s,v_+,\mu,r_2)\,ds \tag{3.5}$$

for $t \in \mathbb{R}_+$ and $Q_+ = I - P_+$, respectively,

$$v_-(t) = \Phi(t,0)\xi + \int_0^t \Phi(t,s)Q_-(s)g(s,v_-,\mu,r_2)\,ds + \int_{-\infty}^t \Phi(t,s)P_-(s)g(s,v_-,\mu,r_2)\,ds \tag{3.6}$$

for $t \in \mathbb{R}_-$ and $P_- = I - Q_-$. It follows by the implicit function theorem in Banach spaces that $v_+ = v_+(\rho,\mu,r_2)$, respectively, $v_- = v_-(\rho,\mu,r_2)$, near the origin. Let $\rho$ be the coordinate in the subspace $U$ and $D = D(\rho,\mu,r_2)$ denote a distance function, which measures the distance

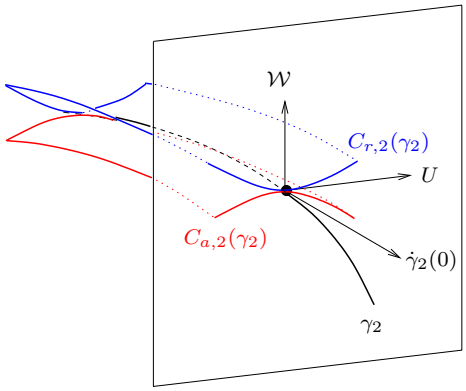


**Figure 11.** *The distance $D(\rho,\mu,r_2)$ between the invariant manifolds $M_{r,2}(r_2)$ and $M_{a,2}(r_2)$ in chart $\kappa_2$ is measured in the subspace $U\oplus\mathcal{W}$ transverse to the special solution $\gamma_2$. Here we show $M_{r,2}(0)=C_{r,2}$ and $M_{a,2}(0)=C_{a,2}$ which have a 2D contact for $\mu\in\mathbb{N}$ along $\gamma_2$.*

between solutions $v_-$ and $v_+$ in a transversal section to the special solution $\gamma_2$ at $t=0$, i.e., in the subspace $U\oplus\mathcal{W}$ (see Figure 11). Then, $D(\rho,\mu,r_2)=0$ denotes the bifurcation equation for solutions of (2.20), which are of at most algebraic growth for $t\to\pm\infty$.

Proposition 3.1 (see [Wec02]). *An analytic expression for the distance function $D$ is given by*

$$D(\rho,\mu,r_2) := \int_{-\infty}^{\infty} \langle \psi(s), g(s, v(\rho,\mu,r_2)(s),\mu,r_2)\rangle\, ds, \tag{3.7}$$

*where $\psi(s)$ is a bounded solution of the adjoint equation (3.2) which decays exponentially in forward and backward time.*

Usually, the bifurcation equation $D(\rho,\mu,r_2)=0$ cannot be solved explicitly. Thus one tries to analyze the equation in the neighborhood of $(0,\mu_0,0)$, $\mu_0\in\mathbb{N}$, with the implicit function theorem or more generally by means of singularity theory (Arnold [Arn81], Golubitsky and Schaeffer [GS84]). For this purpose, we Taylor expand the distance function

$$D(\rho,\mu,r_2) = \frac{\partial D}{\partial\rho}(0,\mu_0,0)\,\rho + \frac{\partial D}{\partial\mu}(0,\mu_0,0)\,(\mu-\mu_0) + \frac{\partial D}{\partial r_2}(0,\mu_0,0)\,r_2 + h.o.t., \tag{3.8}$$

where the partial derivatives of the distance function (3.7) at $(\rho,\mu,r_2)=(0,\mu_0,0)$ are called *Melnikov integrals (Melnikov functions)*. We state our main result.

Theorem 3.1. *For odd $\mu_0$ there exists a transcritical bifurcation of singular canards near $\gamma_2$ in the unperturbed system of (2.13); i.e., the bifurcation equation $D(\rho,\mu,0)=0$ is locally equivalent to the normal form*

$$\rho^2 + (-1)^{\frac{\mu_0+1}{2}}\rho(\mu-\mu_0)=0, \quad \mu_0=2n-1, \quad n\in\mathbb{N}. \tag{3.9}$$

The proof is given in the following by calculating the Melnikov integrals up to second order. For the calculation of the Melnikov integrals, we need an explicit bounded solution $\psi$

of the adjoint equation (3.2) which decays exponentially for $t \to \pm\infty$. The adjoint equation (3.2) can be written as a homogeneous second order differential equation:

$$\psi_1'' + t\psi_1' + (\mu_0 + 1)\psi_1 = 0. \tag{3.10}$$

The transformation $\psi_1(t) = \varphi(t)\exp(-t^2/2)$ brings (3.10) to the Weber equation

$$\varphi'' - t\varphi' + \mu_0\varphi = 0, \tag{3.11}$$

where one solution is given by the Hermite polynomial $H_{\mu_0}(t/\sqrt{2})$ for $\mu_0 \in \mathbb{N}$. Thus the solution $\psi$, which decays exponentially for $t \to \pm\infty$, is given by

$$\begin{pmatrix} \psi_1(t) \\ \psi_2(t) \\ \psi_3(t) \end{pmatrix} = k_1 \begin{pmatrix} H_{\mu_0}(t/\sqrt{2}) \\ \mu_0 H_{\mu_0-1}(t/\sqrt{2})/\sqrt{2} \\ 0 \end{pmatrix} \exp\left(\frac{-t^2}{2}\right), \quad \mu_0 \in \mathbb{N}, \tag{3.12}$$

where

$$k_1 = \begin{cases} \frac{\sqrt{2}}{\mu H_{\mu_0-1}(0)}, & \mu_0 = \text{odd}, \\ \frac{1}{H_{\mu_0}(0)}, & \mu_0 = \text{even}, \end{cases} \tag{3.13}$$

such that $\|\psi(0)\| = 1$. Recall that $\psi(0) \in \mathcal{W}$. Similarly, it follows from (2.24) and $\mu_0 \in \mathbb{N}$ that the transition matrix of the variational equation is of the form

$$\Phi(t,0) = \begin{pmatrix} H_{\mu_0-1}(t/\sqrt{2})/H_{\mu_0-1}(0) & * & 0 \\ -\sqrt{2}H_{\mu_0}(t/\sqrt{2})/(\mu_0 H_{\mu_0-1}(0)) & * & 0 \\ \sqrt{2}H_{\mu_0}(t/\sqrt{2})/(\mu_0 H_{\mu_0-1}(0)) & * & 1 \end{pmatrix}, \quad \mu_0 = \text{odd}, \tag{3.14}$$

$$\Phi(t,0) = \begin{pmatrix} * & -\mu_0 H_{\mu_0-1}(t/\sqrt{2})/(\sqrt{2}H_{\mu_0}(0)) & 0 \\ * & H_{\mu_0}(t/\sqrt{2})/H_{\mu_0}(0) & 0 \\ * & -H_{\mu_0}(t/\sqrt{2})/H_{\mu_0}(0) + 1 & 1 \end{pmatrix}, \quad \mu_0 = \text{even}, \tag{3.15}$$

where $H_0(0) = 1$ and $H_n(0) = (-2)^{n/2}(n-1)!$ for even $n$ (the asterisks denote an unspecified column of the transition matrix). The splitting of the phase-space (3.1) for our Melnikov calculations is given by

$$\mathbb{R}^3 = span\left\{\begin{pmatrix} 0 \\ 0 \\ 1 \end{pmatrix}\right\} \oplus span\left\{\begin{pmatrix} 1 \\ 0 \\ 0 \end{pmatrix}\right\} \oplus span\left\{\begin{pmatrix} 0 \\ 1 \\ 0 \end{pmatrix}\right\}, \quad \mu_0 = \text{odd}, \tag{3.16}$$

$$\mathbb{R}^3 = span\left\{\begin{pmatrix} 0 \\ 0 \\ 1 \end{pmatrix}\right\} \oplus span\left\{\begin{pmatrix} 0 \\ 1 \\ 0 \end{pmatrix}\right\} \oplus span\left\{\begin{pmatrix} 1 \\ 0 \\ 0 \end{pmatrix}\right\}, \quad \mu_0 = \text{even}. \tag{3.17}$$

Lemma 3.1.

$$\frac{\partial D}{\partial \rho}(0, \mu_0, 0) = 0. \tag{3.18}$$

*Proof.* By definition of the function $g(t, v, \mu, r_2)$ (2.22), we have $g(t, 0, \mu_0, 0) = 0$ and

$$\frac{\partial g}{\partial v}(t, 0, \mu_0, 0) = \frac{\partial f}{\partial x}(\gamma_2(t), \mu_0, 0) - A(t, \mu_0) = 0, \tag{3.19}$$

where $x = (x_2, y_2, z_2) \in \mathbb{R}^3$. Hence, it follows immediately that

$$\frac{\partial D}{\partial \rho}(0, \mu_0, 0) = \int_{-\infty}^{\infty} \left\langle \psi(s), \frac{\partial g}{\partial v}(s, 0, \mu_0, 0) \frac{\partial v}{\partial \rho}(0, \mu_0, 0)(s) \right\rangle ds = 0. \qquad \blacksquare$$

This result implies that generically the bifurcation equation cannot be solved for $\rho$ by the implicit function theorem and that a bifurcation of canards occurs.

Lemma 3.2.

$$\frac{\partial D}{\partial \mu}(0, \mu_0, 0) = 0. \tag{3.20}$$

*Proof.* The Melnikov integral is given by

$$\frac{\partial D}{\partial \mu}(0, \mu_0, 0) = \int_{-\infty}^{\infty} \left\langle \psi(s), \frac{\partial f}{\partial \mu}(\gamma_2(s), \mu_0, 0) \right\rangle ds.$$

The result follows immediately from

$$\frac{\partial f}{\partial \mu}(\gamma_2(s), \mu_0, 0) = 0. \qquad \blacksquare \tag{3.21}$$

Lemma 3.3.

$$\frac{\partial^2 D}{\partial \mu^2}(0, \mu_0, 0) = 0. \tag{3.22}$$

*Proof.*

$$\begin{aligned} \frac{\partial^2 D}{\partial \mu^2}(0, \mu_0, 0) = &\int_{-\infty}^{\infty} \left\langle \psi(s), \frac{\partial^2 f}{\partial x^2}(\gamma_2(s), \mu_0, 0) \left( \frac{\partial v}{\partial \mu}(0, \mu_0, 0)(s), \frac{\partial v}{\partial \mu}(0, \mu_0, 0)(s) \right) \right\rangle ds \\ &+ \int_{-\infty}^{\infty} \left\langle \psi(s), \frac{\partial^2 f}{\partial x \partial \mu}(\gamma_2(s), \mu_0, 0) \frac{\partial v}{\partial \mu}(0, \mu_0, 0)(s) + \frac{\partial^2 f}{\partial \mu^2}(\gamma_2(s), \mu_0, 0) \right\rangle ds. \end{aligned} \tag{3.23}$$

The result follows from

$$\left( \frac{\partial f}{\partial \mu}(\gamma_2(s), \mu_0, 0) = 0, \ \frac{\partial g}{\partial v}(t, 0, \mu_0, 0) = 0 \right) \quad \Rightarrow \quad \frac{\partial v}{\partial \mu}(0, \mu_0, 0)(s) = 0 \tag{3.24}$$

and

$$\frac{\partial^2 f}{\partial \mu^2}(\gamma_2(s), \mu_0, 0) = 0. \qquad \blacksquare \tag{3.25}$$

Proposition 3.2.

$$\frac{\partial^2 D}{\partial \rho^2}(0,\mu_0,0) = \begin{cases} \delta_{\rho\rho} \neq 0, & \mu_0 = odd, \\ 0, & \mu_0 = even. \end{cases} \tag{3.26}$$

*Proof.*

$$\frac{\partial^2 D}{\partial \rho^2}(0,\mu_0,0) = \int_{-\infty}^{\infty} \left\langle \psi(s), \frac{\partial^2 f}{\partial x^2}(\gamma_2(s),\mu_0,0)\left(\frac{\partial v}{\partial \rho}(0,\mu_0,0)(s), \frac{\partial v}{\partial \rho}(0,\mu_0,0)(s)\right)\right\rangle ds. \tag{3.27}$$

From the definition of (3.5), respectively, (3.6), it follows that

$$\frac{\partial v}{\partial \rho}(0,\mu_0,0)(s) = \Phi(s,0)\frac{\partial \xi}{\partial \rho}.$$

As the measuring of distance function $D$ just takes place in transverse directions of $\gamma_2(0)$, we set $\xi = \xi(\rho) = \rho u \in U$. Thus

$$\frac{\partial v_\pm}{\partial \rho}(0,\mu_0,0)(s) = \Phi(s,0)u$$

is a solution of at most algebraic growth of the variational equation (2.23). With the splitting of our phase-space (3.16) and definition of the transition matrix (3.14) (resp., (3.17) and (3.15)), we obtain

$$\frac{\partial v}{\partial \rho}(0,\mu_0,0)(s) = \begin{pmatrix} H_{\mu_0-1}(t/\sqrt{2})/H_{\mu_0-1}(0) \\ -\sqrt{2}H_{\mu_0}(t/\sqrt{2})/(\mu_0 H_{\mu_0-1}(0)) \\ \sqrt{2}H_{\mu_0}(t/\sqrt{2})/(\mu_0 H_{\mu_0-1}(0)) \end{pmatrix}, \quad \mu_0 = \text{odd}, \tag{3.28}$$

$$\frac{\partial v}{\partial \rho}(0,\mu_0,0)(s) = \begin{pmatrix} -\mu_0 H_{\mu_0-1}(t/\sqrt{2})/(\sqrt{2}H_{\mu_0}(0)) \\ H_{\mu_0}(t/\sqrt{2})/H_{\mu_0}(0) \\ -H_{\mu_0}(t/\sqrt{2})/H_{\mu_0}(0) + 1 \end{pmatrix}, \quad \mu_0 = \text{even}. \tag{3.29}$$

Using this result and definition (3.12) in (3.27), we get for even $\mu_0$

$$\begin{aligned} \frac{\partial^2 D}{\partial \rho^2}(0,\mu_0,0) &= \frac{\sqrt{2}\mu_0}{H_{\mu_0}^3(0)} \int_{-\infty}^{\infty} H_{\mu_0}(s/\sqrt{2})^2 H_{\mu_0-1}(s/\sqrt{2}) \exp\left(\frac{-s^2}{2}\right) ds \\ &= 0, \end{aligned}$$

respectively, for odd $\mu_0$

$$\begin{aligned} \frac{\partial^2 D}{\partial \rho^2}(0,\mu_0,0) &= \frac{4}{\mu_0^2 H_{\mu_0-1}^3(0)} \int_{-\infty}^{\infty} H_{\mu_0}(s/\sqrt{2})^2 H_{\mu_0-1}(s/\sqrt{2}) \exp\left(\frac{-s^2}{2}\right) ds \\ &= \frac{4}{\mu_0^2 H_{\mu_0-1}^3(0)} \frac{2^{\frac{3\mu_0+1}{2}}(\mu_0!)^3}{(\frac{\mu_0-1}{2}!)^3 \mu_0(\mu_0+1)} \sqrt{2\pi} =: \delta_{\rho\rho}, \end{aligned}$$

which gives the assertion. ∎

Proposition 3.3.

$$\frac{\partial^2 D}{\partial\rho\partial\mu}(0,\mu_0,0) = \delta_{\rho\mu} \neq 0, \quad \mu_0 \in \mathbb{N}. \tag{3.30}$$

*Proof.*

$$\begin{aligned}\frac{\partial^2 D}{\partial\rho\partial\mu}(0,\mu_0,0) = &\int_{-\infty}^{\infty} \left\langle \psi(s), \frac{\partial^2 f}{\partial x^2}(\gamma_2(s),\mu_0,0)\left(\frac{\partial v}{\partial\mu}(0,\mu_0,0)(s), \frac{\partial v}{\partial\rho}(0,\mu_0,0)(s)\right)\right\rangle ds \\ &+ \int_{-\infty}^{\infty} \left\langle \psi(s), \frac{\partial^2 f}{\partial x\partial\mu}(\gamma_2(s),\mu_0,0)\frac{\partial v}{\partial\rho}(0,\mu_0,0)(s)\right\rangle ds.\end{aligned} \tag{3.31}$$

Recall that $\xi = \xi(\rho)$. Thus it follows from definition (3.5), respectively, (3.6) and (3.21), that

$$\frac{\partial v}{\partial\mu}(0,\mu_0,0)(s) = \Phi(s,0)\frac{\partial\xi}{\partial\mu} = 0. \tag{3.32}$$

Using this result and definitions (3.12) and (3.28), respectively, (3.29) in (3.31), we obtain for $\mu_0 \in \mathbb{N}$

$$\begin{aligned}\frac{\partial^2 D}{\partial\rho\partial\mu}(0,\mu_0,0) &= k_2 \int_{-\infty}^{\infty} H(\mu_0, s/\sqrt{2})^2 \exp\left(\frac{-s^2}{2}\right) ds \\ &= k_2\, 2^{\mu_0}\mu_0!\sqrt{2\pi} =: \delta_{\rho\mu},\end{aligned}$$

where

$$k_2 = \begin{cases} -(\mu_0 H_{\mu_0-1}(0))^{-2}, & \mu_0 = \text{odd}, \\ (2H_{\mu_0}^2(0))^{-1}, & \mu_0 = \text{even}. \end{cases} \tag{3.33}$$

■

Singularity theory [GS84] gives then the equivalence of $D(\rho,\mu,0) = 0$ with the normal form (3.9) which is called the recognition problem. The assertion of Theorem 3.1 follows. Note that in the case $\mu = 1$ of the degenerate folded node we have a transcritical bifurcation given by the two special solutions $\gamma_i$, $i = 1, 2$, which we call the primary singular canards. All other bifurcating singular canards we call *secondary*.

*Remark.* To state a similar result for even $\mu_0$ (most likely a pitchfork bifurcation) we would need results on third order Melnikov integrals, but we did not succeed in computing these analytically so far.

**4. Numerical analysis of singular canards.** In the following, we give numerical evidence for the derived transcritical bifurcation for odd $\mu$ and for a pitchfork bifurcation for even $\mu$. Furthermore, we show the existence of a novel turning point bifurcation in a small neighborhood of the transcritical, respectively, pitchfork, bifurcation, i.e., close to $\mu_0 \in \mathbb{N}$. Let $U = \bigcup U_{\mu_0}$ denote the union of neighborhoods of the resonances $\mu_0 \in \mathbb{N}$, where $U_{\mu_0} = (\mu_0 - \rho_0, \mu_0 + \rho_0)$ and $\rho_0$ small. We state the following result on the existence of secondary canards.

Proposition 4.1. *Let $I = (1,\infty)$, $U$ be the union of neighborhoods of the resonances $\mu_o \in \mathbb{N}$ and $\mu \in I/U$. Then system (2.1) possesses $[(\mu-1)/2]$ secondary maximal canards, where $[(\mu-1)/2]$ denotes the greatest integer less than or equal to $(\mu-1)/2$.*

Recall that $C_{a,2}$, respectively, $C_{r,2}$, are the extensions of the invariant manifolds $C_{a,1}$, respectively, $C_{r,1}$, in chart $\kappa_2$ and that singular canards are intersections of $C_{a,2}$ and $C_{r,2}$. A crucial observation of Proposition 2.2 is that $C_{a,1}$, respectively, $C_{r,1}$, is unique for $y_1 > -2(\mu+1)/\mu$, respectively, $y_1 < 2(\mu+1)/\mu$, because the flow is directed away from, respectively, toward, the line of equilibria $L_{a,1}$, respectively, $L_{r,1}$ (saddle property). We fix a curve $\varepsilon_1 = \delta$ of initial conditions in $C_{a,1}$ (resp., $C_{r,1}$) (see Figure 12). Then, there exists a tangency for the flow and the curve of initial conditions at the intersection with the $\varepsilon_1$-nullcline (2.12). We call this point a turning point which is given by

$$TP_{a/r,1} = (\mp 2(\mu+1)/\mu, \mp 1, \delta) = (y_1, z_1, \varepsilon_1). \tag{4.1}$$

All trajectories with initial conditions left of the turning point on $C_{a,1}$, i.e., $y_1 < -2(\mu+1)/\mu$, are folded by the flow onto the trajectories with initial conditions between the turning point and the special solution $\gamma_2$ (see Figure 12). By the time reversing symmetry $\sigma_1$ (2.8), the same holds for trajectories with initial conditions right of the turning point on $C_{r,1}$.

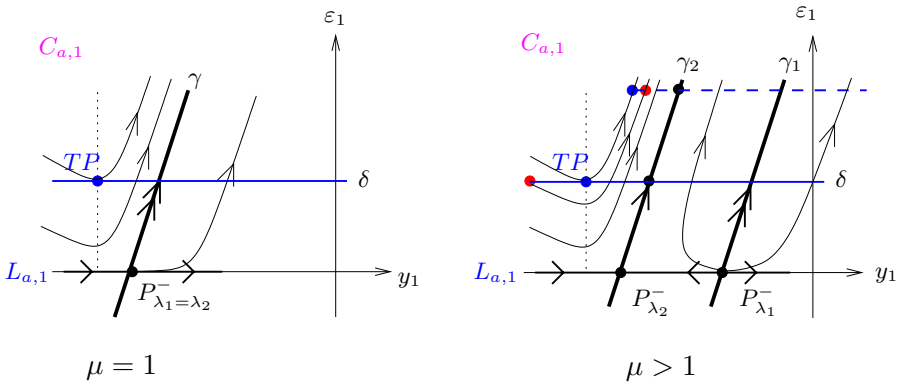


**Figure 12.** *Line of initial conditions on $C_{a,1}$ (solid blue line) and turning point $TP$ (blue circle) of the flow at the intersection with the $\varepsilon_1$-nullcline (dotted line). Trajectories with initial conditions left of the turning point (red circle) are folded under the flow between the trajectory through the turning point and the singular canard $\gamma_2$.*

We follow trajectories with initial conditions between the turning point and the $\varepsilon_1$-axis to obtain a sufficiently global picture of the extension of the manifolds $C_{a,1}$ and $C_{r,1}$ in a neighborhood of the primary canards $\gamma_{1/2}$. This segment of initial conditions is given by

$$IC_{a/r,1} = (\pm y_1, \mp 1 + O(\delta), \delta) = (y_1, z_1, \varepsilon_1) \tag{4.2}$$

with $-2(\mu+1)/\mu \leq y_1 < 0$. The numerical calculations are done in chart $\kappa_2$ for the unperturbed system

$$\begin{aligned} x_2' &= \frac{1}{2}\mu y_2 - (\mu+1)z_2, \\ y_2' &= 1, \\ z_2' &= x_2 + z_2^2 \end{aligned} \tag{4.3}$$

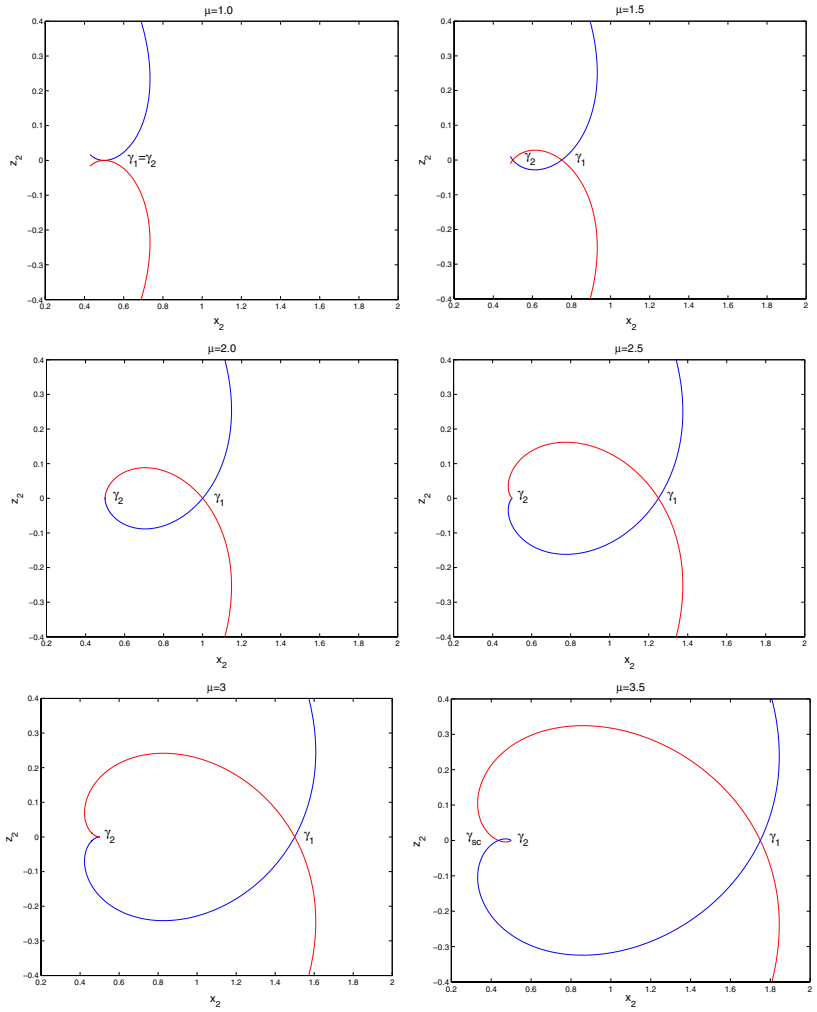


**Figure 13.** *Intersections of manifolds $C_{r,2}$ (blue) and $C_{a,2}$ (red) in cross section $y_2 = 0$ representing singular canards for several values of $\mu$. The primary canards are given by $\gamma_1 = (\mu/2, 0)$ and $\gamma_2 = (1/2, 0)$. Note the appearance of a secondary canard $\gamma_{sc}$ left of $\gamma_2$ for $\mu = 3.5$.*

to show intersections of the invariant manifolds $C_{a,2}$ and $C_{r,2}$. Applying the change of coordinates $\kappa_{21}$ (2.16) to (4.2), we obtain the segment of initial conditions in chart $\kappa_2$

$$IC_{a/r,2} = (-1/\delta, \pm y_2, \sqrt{1/\delta}(\mp 1 + O(\delta))) = (x_2, y_2, z_2) \tag{4.4}$$

with $-2\sqrt{1/\delta}(\mu+1)/\mu \leq y_2 < 0$. Similarly, it follows that the turning point (4.1) is given in chart $\kappa_2$ by

$$TP_{a/r,2} = (-1/\delta, \pm\sqrt{1/\delta}(\mu+1)/\mu, \mp\sqrt{1/\delta}) = (x_2, y_2, z_2). \tag{4.5}$$

We integrate system (4.3) with initial conditions on $IC_{a,2}$ in forward time until trajectories cross the plane $y_2 = 0$, which is a transverse section for the flow because $y_2$ is simply the

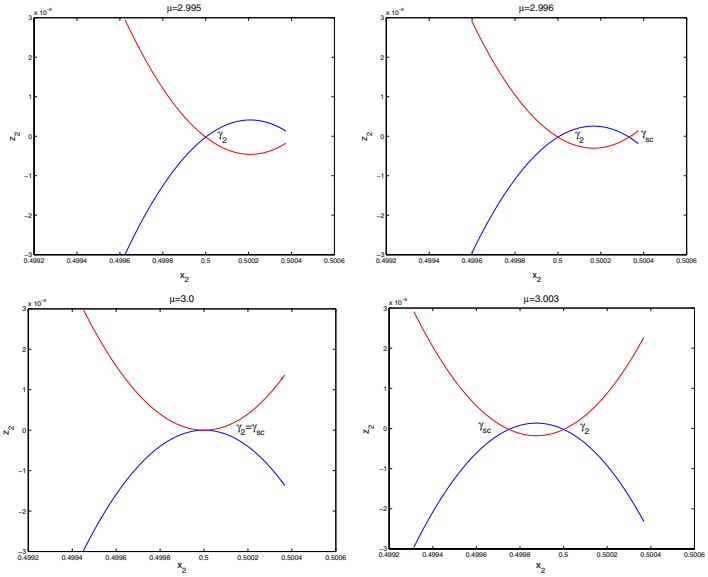


**Figure 14.** *Intersection of manifolds $C_{r,2}$ (blue) and $C_{a,2}$ (red) in cross section $y_2 = 0$ representing singular canards. There is a transcritical bifurcation at $\mu = 3$ between the primary canard $\gamma_2 = (1/2, 0)$ and the secondary canard $\gamma_{sc}$. Furthermore, a "turning point bifurcation" is observed for $2.995 < \mu < 2.996$ which creates the secondary canard $\gamma_{sc}$.*

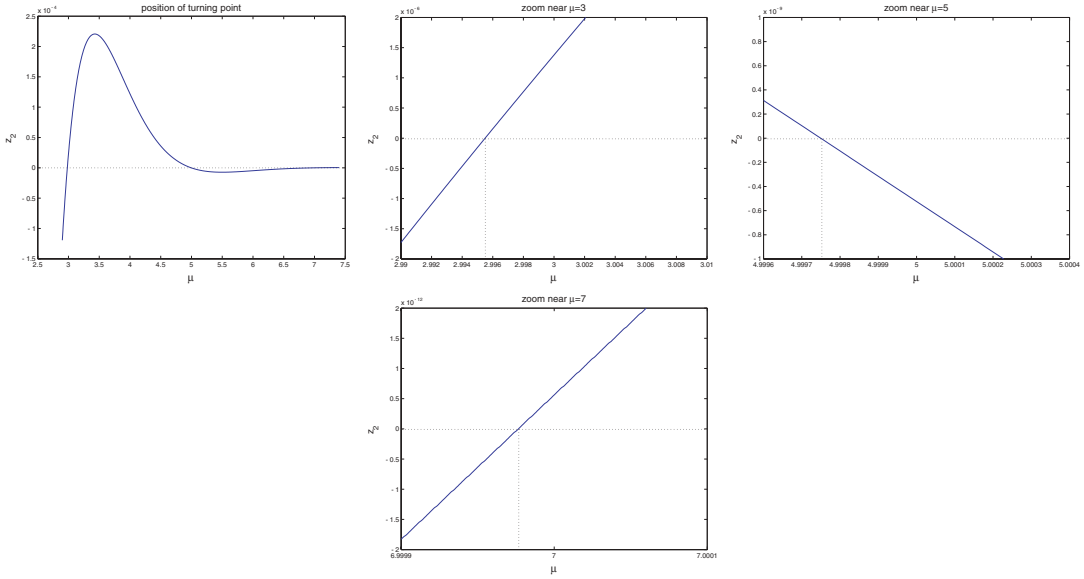


**Figure 15.** *Position of turning point in cross section $y_2 = 0$ as a function of the parameter $\mu$. A turning point bifurcation is observed when the turning point crosses $z_2 = 0$, e.g., at $\mu \approx 2.995$, $\mu \approx 4.9998$, and $\mu \approx 6.99998$.*

time $t_2$ for system (4.3). We also integrate system (4.3) with initial conditions on $IC_{r,2}$ in backward time until trajectories cross the plane $y_2 = 0$. Obviously, singular canards are

intersection points of $(y_2 = 0) \cap (C_{r,2} \cap C_{a,2})$. Note that the primary canards $\gamma_{1/2}$ (2.15) are given in the plane $y_2 = 0$ by

$$(y_2 = 0) \cap \gamma_1 = (\mu/2, 0) = (x_2, z_2),$$
$$(y_2 = 0) \cap \gamma_2 = (1/2, 0) = (x_2, z_2).$$

Furthermore, system (4.3) possesses the time reversing symmetry

$$\sigma_2(x_2, y_2, z_2, t_2) = (x_2, -y_2, -z_2, -t_2), \tag{4.6}$$

which recovers the time reversing symmetry $\sigma_1$ (2.8) in chart $\kappa_1$. It follows by the time reversing symmetry property (4.6) that the image of the initial conditions $IC_{a,2}$ in $y_2 = 0$ obtained by integrating system (4.3) in forward time is the same as the reflection of the image of the initial conditions $IC_{r,2}$ in $y_2 = 0$ obtained by integrating system (4.3) in backward time with the $x_2$-axis as the axis of reflection; i.e., $(y_2 = 0) \cap C_{a,2}$ is the reflection of $(y_2 = 0) \cap C_{r,2}$ with $z_2 \mapsto -z_2$.

We fix $\delta = 1/100$ in (4.4) for all our numerical integrations using a fourth order Runge–Kutta method. Figure 13 shows the intersections of $C_{r,2}$ (blue) and $C_{a,2}$ (red) for several values of $\mu$. We observe the tangencies of the invariant manifolds $C_{r,2}$ and $C_{a,2}$ at $\gamma_2$ for $\mu \in \mathbb{N}$ as well as the transverse intersection for $\mu \notin \mathbb{N}$ stated in Proposition 2.4. Note the bifurcating primary (strong) canard $\gamma_1$ with its robust transverse intersection of $C_{r,2}$ and $C_{a,2}$ stated in Proposition 2.3. Furthermore, a secondary canard has bifurcated from $\gamma_2$ for $\mu \geq 3$.

Figure 14 shows a close-up of the invariant manifolds near $\gamma_2$ close to the transcritical bifurcation at $\mu = 3$. Note the short branches of the invariant manifolds. The tip of each branch is the image of the trajectory with the turning point $TP_{a/r,2}$ as initial condition. The manifold $C_{r,2}$ respectively, $C_{a,2}$, do not end at the tip but get folded back onto the branch between the tip and the primary canard $\gamma_2$ (see Figure 12 for an explanation). Because of this folding back mechanism, we observe another bifurcation of secondary canards at $\mu \approx 2.995$. We call this bifurcation a *turning point bifurcation* (TPB).

By the symmetry properties given by $\sigma_2$ (4.6), the turning point bifurcation happens when the turning point crosses the $x_2$-axis in the cross section $y_2 = 0$. Figure 15 shows a graph of the turning point position over the parameter $\mu$ in $y_2 = 0$. The first three bifurcation values close to $\mu = 3, 5, 7$ can be seen. These two bifurcations, the transcritical and turning point bifurcations, are always observed near an odd $\mu$.

Figure 16 shows a numerically observed pitchfork bifurcation at $\mu = 2$, where the bifurcating branches exist for $\mu < 2$. Again, we observe close by a turning point bifurcation for $\mu \approx 1.999$. Thus the two secondary canards which bifurcate from $\mu = 2$ exist just for a tiny parameter interval. Again, these two bifurcations, the pitchfork and turning point bifurcations, are always observed near an even $\mu$. Hence, we have an alternation of transcritical and pitchfork bifurcation for $\mu \in \mathbb{N}$ with nearby turning point bifurcation.

In Figure 17, we summarize these partly analytical, partly numerical results in a bifurcation diagram for (the extensions of) singular canards in chart $\kappa_2$. This gives a complete picture of the existence of secondary singular canards.

Note that the primary canard $\gamma_2$ serves as an organizing center for the rotation of the invariant manifolds $C_{r,2}$, respectively, $C_{a,2}$. Their rotation number increases monotonically

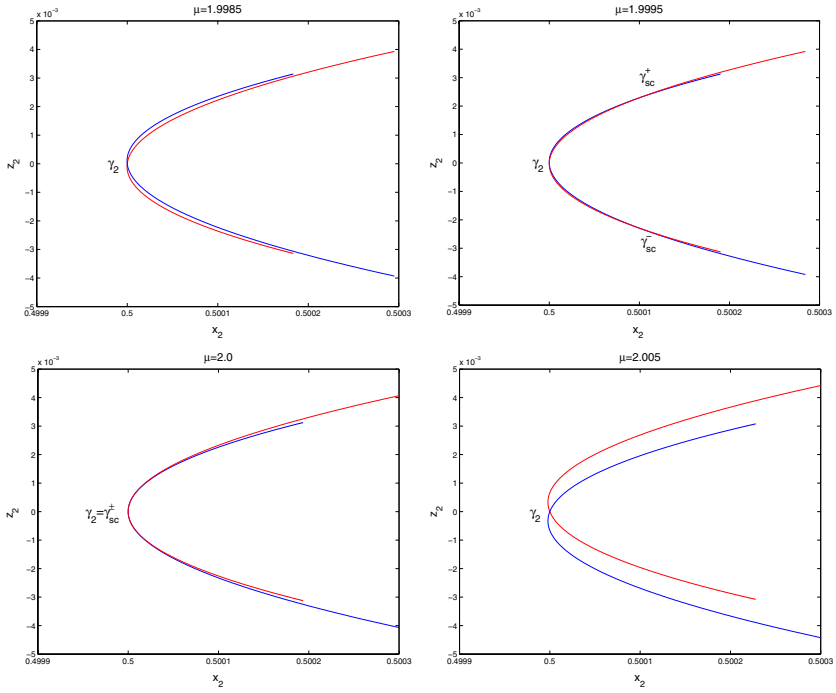


**Figure 16.** *Intersection of manifolds $C_{r,2}$ (blue) and $C_{a,2}$ (red) in cross section $y_2 = 0$ representing singular canards. There is a pitchfork bifurcation at $\mu = 2$ between the primary canard $\gamma_2 = (1/2, 0)$ and the secondary canards $\gamma_{sc}^{\pm}$. Furthermore, a "turning point bifurcation" is observed for $1.9985 < \mu < 1.9995$ which creates the secondary canards $\gamma_{sc}^{\pm}$.*

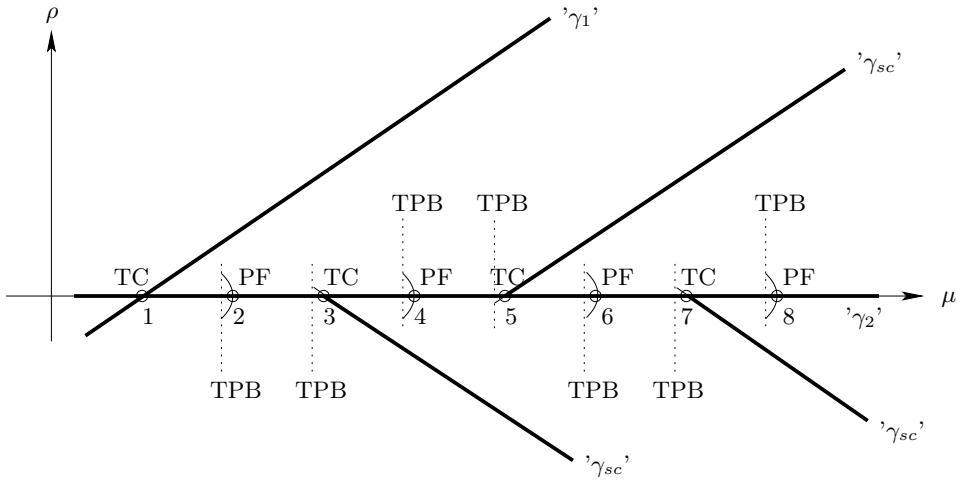


**Figure 17.** *Bifurcation diagram for singular canards in $\kappa_2$: Transcritical (TC), pitchfork (PF), and turning point (TPB) bifurcations; primary canards $\gamma_{1/2}$, secondary canards $\gamma_{sc}$; distance $\rho$ with respect to primary canard $\gamma_2$.*

with $\mu$. A secondary canard bifurcates for $\mu \geq \mu_0$, where $\mu_0$ is odd, and is positioned between the two primary canards $\gamma_1$ and $\gamma_2$. This secondary canard $\gamma_{sc}$ rotates $\mu_0$ times around $\gamma_2$. Furthermore, a secondary canard does not change its rotation properties after bifurcation with increasing $\mu$. It is "released" from the organizing center $\gamma_2$ but "captured" by the stable primary canard $\gamma_1$, respectively, previously bifurcated secondary canards. All these secondary canards are well separated by a rotation angle of $2\pi$ due to the monotonically increasing rotation number of the organizing center. Thus they cannot be annihilated or create new canards by interactions; i.e., there are no more bifurcations.

Another observation which distinguishes secondary canards from primary canards besides their rotational properties is the following. On the blown-up sphere, the secondary singular canards $\gamma_{sc}$ originate from the node $P^-_{\lambda_1}$ in $C_{a,1}$ as well as the primary singular canard $\gamma_1$ (see Figure 18). But on the blown-up critical manifold $S_{a,1}$ the sector of singular canards is attracted to $P^-_{\lambda_2}$. Therefore, the secondary singular canards coalesce with the unique trajectory corresponding to the strong primary canard in $S_{a,1}$, respectively, $S_{r_1}$; i.e., in the "blown-down" system (2.1) the secondary canards converge to the primary strong canard in the singular limit $\varepsilon \to 0$. For small perturbations $0 < \varepsilon \ll 1$, the secondary canards become "visible" and are separated from the primary canards as shown by the preceding blow-up analysis.

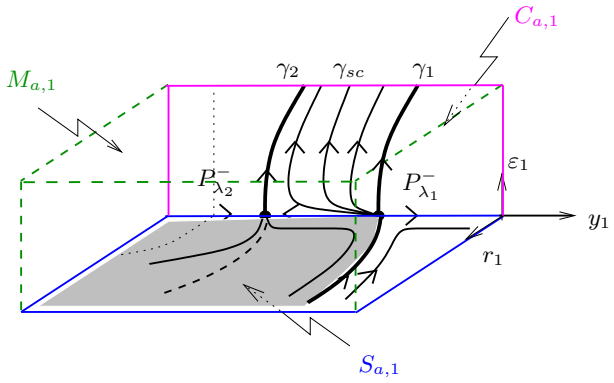


**Figure 18.** *Secondary singular canards $\gamma_{sc}$ on invariant manifold $C_{a,1}$ for, e.g., $\mu = 8.5$.*

The unfolding under small perturbations of the bifurcation diagram (Figure 17) depends on the higher order terms $O(r_2)$ in (2.13). The unfolding of transcritical and pitchfork bifurcation is well covered by singularity theory, but the unfolding of the turning point bifurcation is not known, and complex behavior and interaction with the nearby bifurcation points is expected. We are not addressing this subtle issue in this work. The only conclusion we make in this general setting is the following. There exist no branches of secondary singular canards outside a neighborhood of a pitchfork bifurcation, and there exists just one branch of secondary singular canards outside a neighborhood of a transcritical bifurcation. Recall that $U$ denotes the union of neighborhoods $U_{\mu_0}$ of the bifurcation points $\mu_0 \in \mathbb{N}$. Outside $U$, the branches of secondary canards of the transcritical bifurcations exist and the associated manifolds $C_{r,2}$ and $C_{a,2}$ have a transverse intersection along these secondary canards. Hence, they persist as maximal secondary canards under small perturbations. The assertion of Proposition 4.1 follows. We give numerical evidence of the statement for $\mu = 8.5$ in Figure 19 and for $\mu = 14.5$

in Figure 20. Furthermore, we observe the rotational properties of the invariant manifolds stated in Proposition 2.5.

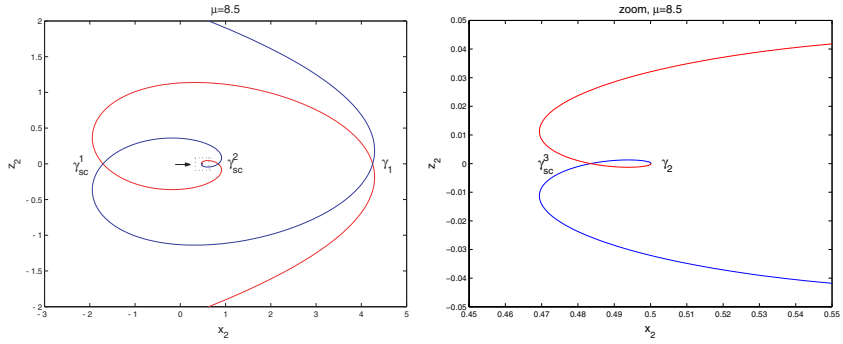


**Figure 19.** *Intersection of manifolds $C_{r,2}$ (blue) and $C_{a,2}$ (red) in cross section $y_2 = 0$ for $\mu = 8.5$ representing the two primary canards $\gamma_1$–$\gamma_2$ and three secondary canards $\gamma_{sc}^1$–$\gamma_{sc}^3$ (the arrow indicates the zoom).*

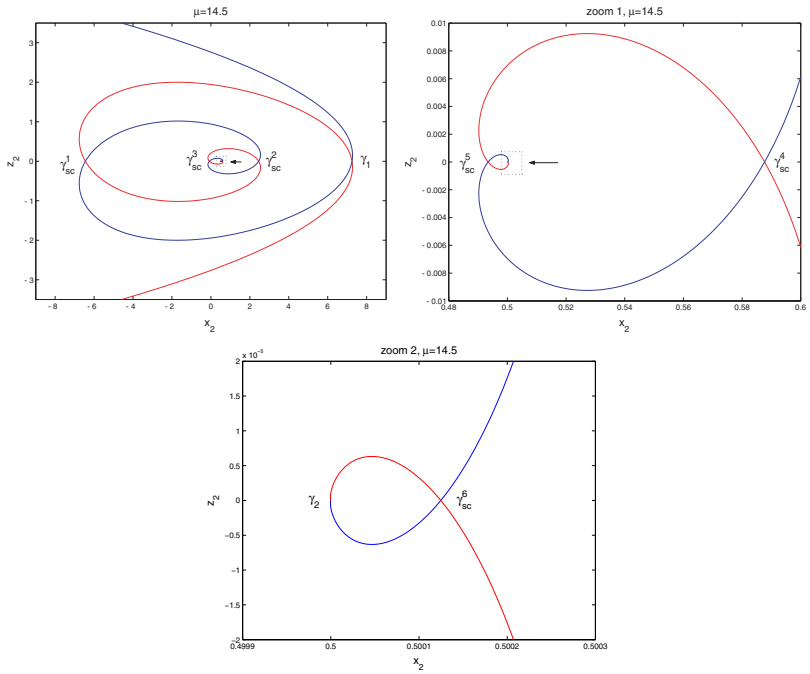


**Figure 20.** *Intersection of manifolds $C_{r,2}$ (blue) and $C_{a,2}$ (red) in cross section $y_2 = 0$ for $\mu = 14.5$ representing the two primary canards $\gamma_1$–$\gamma_2$ and six secondary canards $\gamma_{sc}^1$–$\gamma_{sc}^6$ (the arrows indicate two consecutive zooms).*

**5. Canards in a synchronized network of Hodgkin–Huxley neurons.** Drover et al. [DRSE04] studied numerically a network of Hodgkin–Huxley (HH) neurons [HH52] which are coupled by excitatory synapses. The individual neurons are intrinsically active (e.g., through current injection) with a high firing rate of about 100 Hz. After the synaptic coupling is turned

on, the network rapidly synchronizes and fires at a frequency of only about 10 Hz. Stronger coupling, i.e., a higher synaptic conductance, or a longer decay rate of the synapses lead to even lower frequencies. We will show here that canards of folded node type are responsible for this phenomenon.

The synchronization of the network is partly due to the phase response properties of HH neurons [HMM95]. Furthermore, the extreme slowing observed in the HH network also contributes to the synchronization through a form of fast threshold modulation [SK93]. Since synchrony appears to be a stable state of the network [DRSE04], it is sufficient to study a single self-coupled HH neuron. The network contains only three currents: a transient sodium current, a potassium current (delayed rectifier), and a leak current. A standard procedure reduces the four variable HH model to a two variable reduced HH model (see, e.g., [Rin85]). The resulting single self-coupled reduced HH neuron is given by

$$\begin{aligned} C\,V' &= -g_{Na}\,h\,m_\infty^3(V)(V-V_{Na}) - g_K\,n^4(h)(V-V_K) - g_L(V-V_L) \\ &\quad + g_{syn}s(V-V_{syn}) + I_{app}, \\ h' &= (h_\infty(V)-h)/\tau_h(V), \\ s' &= \alpha(V)(1-s) - s/\tau_{syn}, \end{aligned} \tag{5.1}$$

with voltage $V$, $h \in [0,1]$ the inactivation of the sodium channels, and $s \in [0,1]$ the synaptic coupling. For the definitions of the parameters and functions in (5.1), we refer to Appendix A of [DRSE04].

Figure 21 shows the phenomenon of lowering the frequency from approximately 100 Hz to 10 Hz due to the synaptic coupling in a simulation of the HH neuron (5.1) with a decay rate of the synapse $\tau_{syn} = 10$ ms. Note the occurrence of small oscillations before the neuron fires an action potential. Furthermore, there is a rebound of the voltage after the neuron fires an action potential. We will show that a canard causes the delay of the firing rate by preventing the neuron from firing successive action potentials.

An important observation is that the decay rate $\tau_{syn}$ of the synapse $s$ and the decay rate $\tau_h(V)$ of the inactivation of the sodium channel $h$ are of the same order (5–10 ms). The evolution of $h$ and the deactivation of $s$ are slow compared to the evolution of the voltage $V$ ($C = 1$ in (5.1)). Thus system (5.1) can be viewed as a singularly perturbed system with 2 slow variables and 1 fast variable.

In the following, we study a FitzHugh–Nagumo (FHN) model [FiH60, NAY62], which has the same qualitative features as the reduced HH neuron of (5.1); i.e., in the phase plane both models have a cubic shaped V-nullcline (critical manifold) and an equilibrium close to the lower fold on the repelling middle branch; i.e., the uncoupled neuron is in an oscillatory state and fires action potentials. The FHN model is a simpler model in dimensionless form and is thus easier to analyze. The self-coupled FHN model used here is

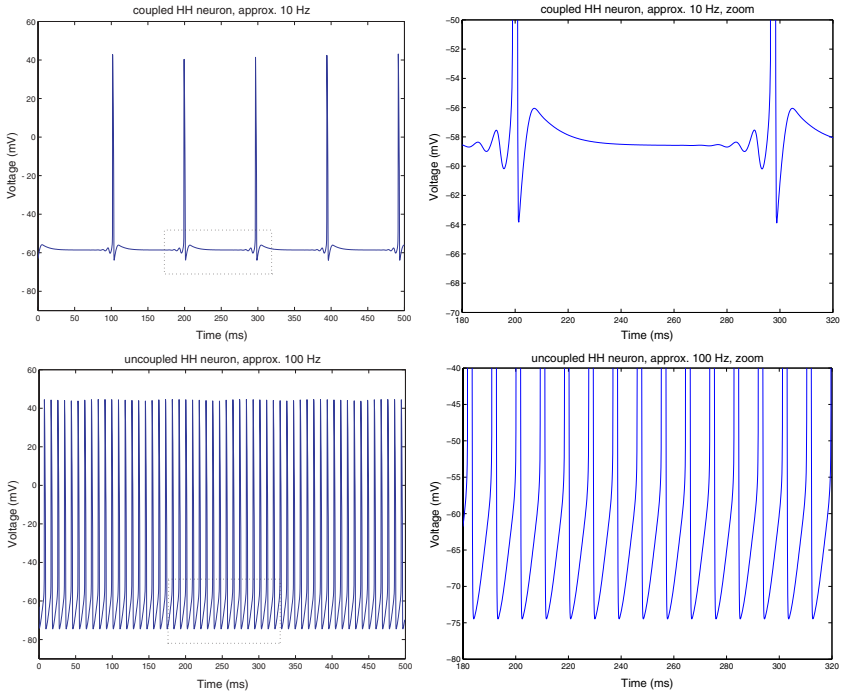


**Figure 21.** *Simulation of HH neuron (5.1) with excitatory synapse (self-coupled); the decay rate of the (slow) synapse is $\tau_{syn} = 10$ ms. The uncoupled neuron fires with about 100 Hz, while the self-coupled neuron fires with about 10 Hz.*

$$\begin{aligned} v' &= h - (v^3 - v + 1)/2 - \gamma s v, \\ h' &= -\varepsilon(2h + 2.6v), \\ s' &= \beta H(v)(1 - s) - \varepsilon\delta s, \end{aligned} \tag{5.2}$$

where $H(v)$ is the Heaviside function, $\gamma$ the coupling strength, $\beta$ the activation rate, $\varepsilon\delta$ the decay rate of the synapse, and $\varepsilon \ll 1$ the singular perturbation parameter. Note that we have substituted the function $\alpha(V)$ in (5.1) by $\beta H(v)$ in (5.2), which is a well-known approximation in synaptic models [RT02]. Thus the synapse $s$ is slow in the silent phase $v < 0$, while it is fast in the active phase $v > 0$. This reflects the physiological property of a slow synapse. Figure 22 shows a simulation of the FHN neuron which shows qualitatively the same behavior as the HH neuron in Figure 21.

To understand the slowing of the firing rate, we have to study the FHN neuron in the silent phase $v < 0$, where the model is given by

$$\begin{aligned} v' &= h - (v^3 - v + 1)/2 - \gamma s v, \\ h' &= -\varepsilon(2h + 2.6v), \\ s' &= -\varepsilon\delta s, \end{aligned} \tag{5.3}$$

which is of the form (1.5) and fits our framework. The critical manifold $S$ of system (5.3) is

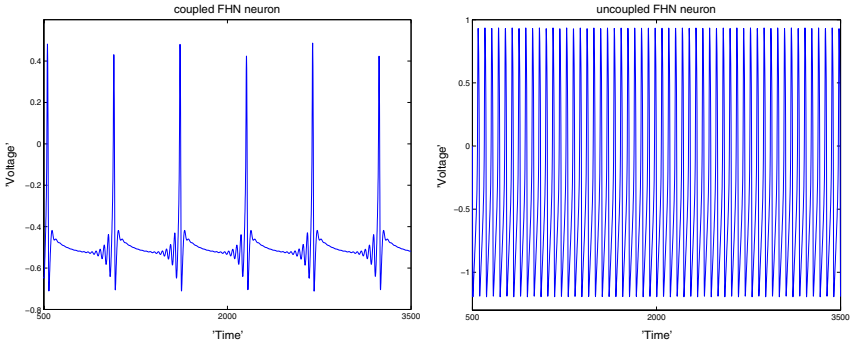


**Figure 22.** *Simulation of FHN neuron (5.2) with excitatory synapse (self-coupled); the activation rate of the synapse is $\beta = 0.2$, the (slow) decay rate of the synapse is $\delta = 0.6$, the synaptic coupling strength is $\gamma = 0.5$, and the singular perturbation parameter is $\varepsilon = 0.015$. The uncoupled neuron ($\gamma = 0$) fires about 10 times faster than the self-coupled neuron.*

given by

$$h = \varphi(v, s) = (v^3 - v + 1 + 2\gamma s v)/2, \tag{5.4}$$

which is a folded manifold (like Figure 2) for $v < 0$, $s \in (0, 1)$, and $\gamma < 0.5$.

*Remark.* Drover et al. [DRSE04] analyzed a similar model for the silent phase, but the synapse $s$ is not explicitly evolving on a slow time scale. Furthermore, they focus on the evolution of the variables $(v, h)$ and view the synapse $s$ like a parameter instead of a second slow variable. This is mainly because they are comparing their results with the classical 2D literature on delayed Hopf bifurcation and canards.

The desingularized reduced system of (5.3) is given by

$$\begin{aligned} \dot{v} &= -(v^3 - v + 1 + 2\gamma s v) - 2.6v + \gamma\delta v s, \\ \dot{s} &= -\delta s(3v^2 - 1 + 2\gamma s)/2. \end{aligned} \tag{5.5}$$

We are looking for singularities of system (5.5) on the fold-curve $L$, given by

$$s = \psi(v) = (1 - 3v^2)/2\gamma \tag{5.6}$$

for $v < 0$ and $0 < s < 1$. This leads to solving the cubic equation

$$(3\delta/2 - 2)v^3 + (2.6 - \delta/2)v + 1 = 0.$$

This equation has for all $\delta \geq 0$ a real solution $v < 0$ such that $0 \leq \psi(v) \leq \bar{s}_\gamma$, where $\bar{s}_\gamma < 1$ for $\gamma > \bar{\gamma} \approx 0.185$. Figure 23 shows for fixed coupling strength $\gamma = 0.5$ the coordinates $(s, v)$ of the singularity.

Computing the parameter $\mu$ shows that these singularities are canard points of folded node type for $0 \leq \delta < \bar{\delta}(\gamma)$ with, e.g., $\bar{\delta}(0.5) \approx 8.72$. Thus the theory of the previous sections applies to this problem.

*Remark.* We want to point out that it is not necessary to transform system (5.3) to the canonical form (2.1) to calculate the parameter $\mu$. Simply calculate the eigenvalues $\lambda_{1/2}$ of the

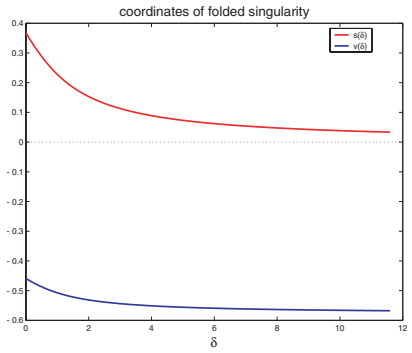


**Figure 23.** *Coordinates of the folded singularity in the reduced problem for coupling strength $\gamma = 0.5$ as a function of the synaptic decay rate $\delta$ (obtained analytically by Maple).*

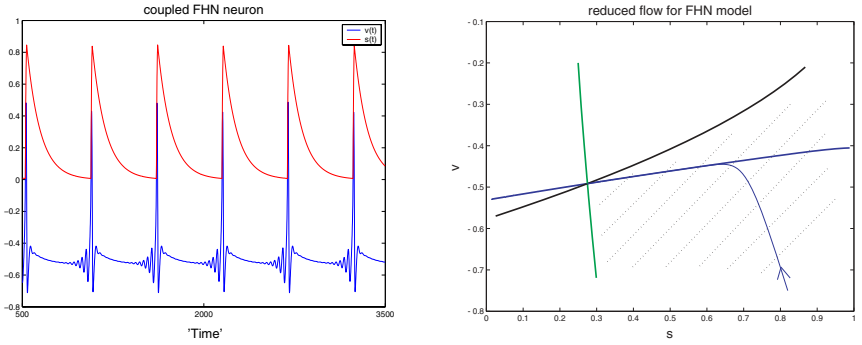


**Figure 24.** *Left: Evolution of $s$ (red) and $v$ (blue) of the FHN model (5.2) with same parameters as in Figure 22. Right: Reduced flow (blue) near singularity of folded node type, primary strong canard (bold green), primary weak canard (bold blue), fold-curve (black), and sector of weak canards (dotted area).*

singularities of system (5.5) to obtain $\mu = \lambda_1/\lambda_2$. Eigenvalues are invariant under coordinate transformations.

Figure 24 shows the evolution of the synapse $s$ and the voltage $v$. Note that resetting the synapse to a value $s \approx 0.8$ after an action potential occurs, which is due to the fast dynamics in the active phase. Furthermore, Figure 24 shows the associated reduced flow near the fold-curve in the silent phase. A trajectory enters the silent phase inside the sector between the two primary canards of the folded node (dotted area). From Proposition 4.1 follows the existence of $[(\mu - 1)/2]$ secondary weak canards within the dotted sector (in this case, $\mu \approx 52 \Rightarrow [(52 - 1)/2] = 25$ secondary canards). Furthermore, $\mu \approx 52$ denotes the ratio between the eigenvalues of the folded node singularity; i.e., the strong eigendirection is approximately 52 times stronger than the weak eigendirection. Thus a trajectory which enters the silent phase in the dotted sector gets quickly attracted to the primary weak canard. This explains the rebound of the voltage after an action potential is fired. The primary weak canard prevents the neuron from reaching the threshold (fold-curve) to fire an action potential. Instead the trajectory follows the primary canard and passes close to the canard point near the fold-curve to the repelling manifold.

Furthermore, the numerical analysis in section 4 showed that the attracting and repelling manifold form a "funnel" along the primary weak canard (see Figures 19–20). Note that the secondary canards divide the sector of weak canards into $([(\mu-1)/2]+1) = 26$ subsectors. Thus depending on the initial subsector of the trajectory, the trajectory has to rotate around the primary weak canard for some time before it gets repelled and finally fires an action potential. This explains the observed subthreshold oscillations. The paradox that a neuron has to hyperpolarize to reach the action potential threshold is well explained by the shape of the fold-curve (the action potential threshold) and the primary weak canard in the phase plane (Figure 24). This firing behavior is robust and explains qualitatively the observed delay in the firing of the FHN neuron (5.2), respectively, the HH neuron (5.1).

*Remark.* This folded node structure embedded in the FHN neuron explains the "novel vortex structure" observed by Drover et al. [DRSE04].

We want to point out that the periodic patterns created by the canards of folded node type in the FHN, respectively, HH, model are mixed mode oscillations (MMOs) [PPS92], for which the oscillatory cycle consists of a number of large amplitude oscillations and a number of small amplitude oscillations. This becomes more apparent in our model, if the resonance parameter $\mu$ is not so large. Figure 25 shows $1^0$–$1^5$ MMO patterns where $\mu \approx 9.9$ for all six patterns, where the parameters corresponding to the silent phase are fixed. We are just varying the activation rate $\beta$ of the synapse. Thus we are changing the "initial condition" for the trajectory entering the silent phase. We have four secondary canards which divide the sector between the two primary canards into five subsectors (see Figure 26). For small values of the activation rate $\beta$, we enter the silent phase to the left of the primary strong canard (outside the sector), and we are in the relaxation regime which corresponds to the MMO pattern $1^0$. With increasing $\beta$, trajectories enter the subsectors between the primary strong canard and the primary weak canard. Remember that the secondary canards are well separated by a rotation angle of $2\pi$. Thus depending on the subsector where the trajectory is initially positioned we obtain $1^1$–$1^5$ MMO patterns. These patterns are generically robust under small perturbations. Just in the transition from one subsector to another, chaotic behavior has to be expected. A detailed study of MMO patterns in systems with folded nodes is part of future work.

*Remark.* Another class of problems where MMOs occur are systems with canard points of folded saddle-node type (type II). A geometric analysis for this class of MMO can be found in [MSLG98], where Milik et al. studied a 3D chemical autocatalator, and in [BKW04].

**6. Conclusion.** In this paper, we have studied the complicated dynamics of slow-fast systems associated with the occurrence of folded node singularities. We have used geometric singular perturbation theory, the blow-up technique, and an extension of Melnikov theory to show the existence of secondary canards, which is due to a transcritical bifurcation of the attracting and repelling invariant manifolds along the primary weak canard whenever the resonant parameter $\mu$ passes through an odd number. For practical purposes, another important insight is that all solutions within the sector of the primary canards observe a delay effect. This is due to the rotational properties of the invariant manifolds near the primary weak canard which leads to a "funnel" effect. Solutions are trapped within this funnel for a certain amount of time observing a delay of repulsion. This geometric property is robust under perturbation and thus can be easily observed as shown in the analysis of the HH

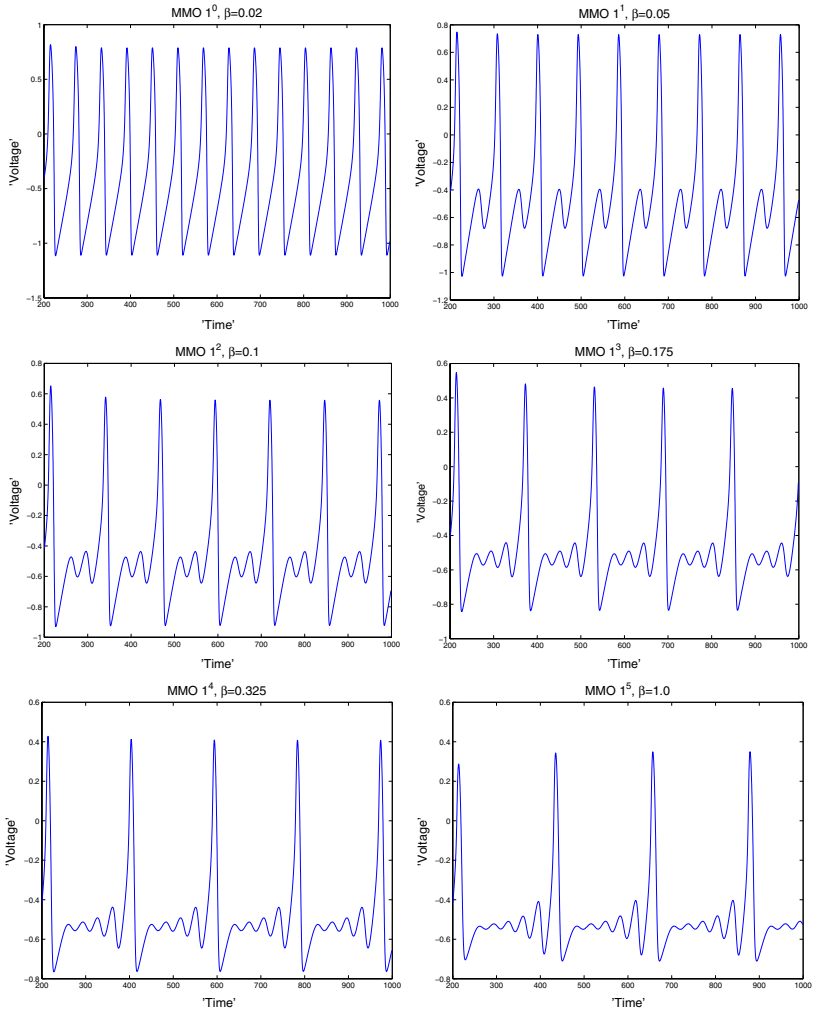


**Figure 25.** *MMOs with* $1^0$–$1^5$ *pattern in the FHN model* (5.2) *obtained by variation of activation rate* $\beta$. *Same parameter values as in Figure* 22 *but* $\delta = 3$.

network. Furthermore, we have pointed out that this delay effect of firing is closely related to MMOs which are widely observed in chemical oscillators. In our case, the MMO patterns are of the form $1^N$, where $N$ denotes the number of subthreshold oscillations, which is related to the number of secondary canards.

From the experimental point of view, we want to emphasize that canards are generic objects in systems with two or more slow variables like in the FHN model in the silent phase (5.3). They are robust and have a certain impact on the dynamics of the underlying problem. In particular, the above described funnel effect of canards of folded node type should be easily observed in real experiments. We also want to point out that this effect cannot be appropriately explained in a 2D system where canards are degenerate. If a model exhibits more than one slow variable, then a reduction to just one slow variable is in most cases not desirable.

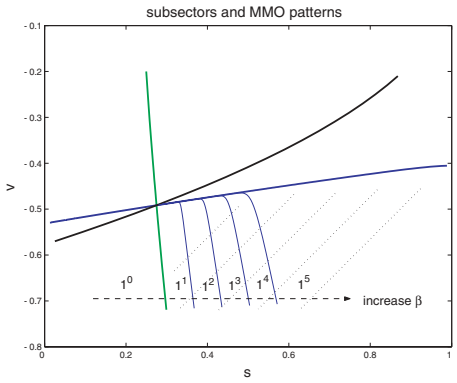


**Figure 26.** *Secondary canards (blue), primary strong canard (bold green), primary weak canard (bold blue), fold-curve (black), and sector of weak canards (dotted area). Secondary canards divide sector into subsectors which represent the domains of the MMO patterns* $1^1$–$1^5$ *of Figure* 25.

Mathematically, the analysis of canards in $\mathbb{R}^3$ (of folded node type) is pinned down to intersections of the invariant manifolds $S_{a,\varepsilon}$ and $S_{r,\varepsilon}$ and their slow dynamics. The main part of this analysis is done in chart $\kappa_2$ of the blow-up which covers the dynamics on the blown-up sphere $S^3$. By using Melnikov theory and numerical analysis, we have obtained more insight into the dynamics of these manifolds. In particular, we have a better understanding of the unperturbed system $\{(4.3),\ r_2 = 0\}$, which can be written as a second order nonlinear inhomogeneous equation

$$z'' - 2zz' + (\mu + 1)z = \frac{1}{2}\mu t. \tag{6.1}$$

This equation serves like a normal form of the underlying problem, similarly to the classical Riccati equation in the case of a regular fold (without canard points). Understanding the dynamics of (6.1) is the main step in solving the canard problem. Our analysis showed that (6.1) possesses besides the two explicitly known solutions $\gamma_{1/2}$ (2.15) further $[(\mu - 1)/2]$ solutions $\gamma_{sc}$ which are of at most algebraic growth. Furthermore, our analysis provided an insight into the rotational properties of the invariant manifolds $\bar{C}_a$ and $\bar{C}_r$, which are the extensions of the attracting and repelling slow manifolds $\bar{S}_a$ and $\bar{S}_r$ on the blown-up sphere (Figure 10). There is still much to explore, especially the observed folding back mechanism of the manifolds $\bar{C}_a$ and $\bar{C}_r$. A more detailed tracking of these manifolds in forward and backward time should give a better understanding of this phenomenon and of the observed turning point bifurcation of secondary canards.

**Acknowledgments.** I would like to thank John Guckenheimer, Martin Krupa, and Peter Szmolyan for carefully and critically reading the manuscript and the referees for all their useful suggestions. Furthermore, I am indebted to Nancy Kopell who encouraged me to include the section on coupled Hodgkin–Huxley neurons in this work.

## REFERENCES


[Arn81] V. I. Arnold, *Singularity Theory*, London Math. Soc. Lecture Note Ser. 53, Cambridge University Press, Cambridge, UK, 1981.

[BCDD81] E. Benoît, J. F. Callot, F. Diener, and M. Diener, *Chasse au canard*, Collect. Math., 31–32 (1981), pp. 37–119.

[Ben83] E. Benoît, *Systèmes lents-rapides dans* $\mathbb{R}^3$ *et leur canards*, Astérisque, 109–110 (1983), pp. 159–191.

[Ben90] E. Benoît, *Canards et enlacements*, Inst. Hautes Études Sci. Publ. Math., 72 (1990), pp. 63–91.

[Ben01] E. Benoît, *Perturbation singuliére en dimension trois: Canards en un point pseudo-singulier noeud*, Bull. Soc. Math. France, 129 (2001), pp. 91–113.

[BEG03] K. Bold, C. Edwards, J. Guckenheimer, S. Guharay, K. Hoffman, J. Hubbard, R. Oliva, and W. Weckesser, *The forced van der Pol equation* II: *Canards in the reduced system*, SIAM J. Appl. Dyn. Syst., 2 (2003), pp. 570–608.

[BCE97] V. Booth, T. W. Carr, and T. Erneux, *Near-threshold bursting is delayed by a slow passage near a limit point*, SIAM J. Appl. Math., 57 (1997), pp. 1406–1420.

[BB91] M. Brøns and K. Bar-Eli, *Canard explosion and excitation in a model of the Belousov-Zhabotinskii reaction*, J. Phys. Chem., 95 (1991), pp. 8706–8713.

[BKW04] M. Brøns, M. Krupa, and M. Wechselberger, *Mixed Mode Oscillations and Canards of Folded Saddle-Node Type*, in preparation, 2004.

[BDE95] F. Buchholtz, M. Dolnik, and I. R. Epstein, *Diffusion-induced instabilities near a canard*, J. Phys. Chem., 99 (1995), pp. 15093–15101.

[Die84] M. Diener, *The canard unchained or how fast/slow dynamical problems bifurcate*, Math. Intelligencer, 6 (1984), pp. 38–49.

[DRSE04] J. Drover, J. Rubin, J. Su, and B. Ermentrout, *Analysis of a canard mechanism by which excitatory synaptic coupling can synchronize neurons at low firing frequencies*, SIAM J. Appl. Math., 65 (2004), pp. 69–92.

[DR96] F. Dumortier and R. Roussarie, *Canard cycles and center manifolds*, Mem. Amer. Math. Soc., 557 (1996).

[Eck83] W. Eckhaus, *Relaxation oscillations including a standard chase on French ducks*, in Asymptotic Analysis II, Lecture Notes in Math. 985, Springer-Verlag, New York, 1983, pp. 449–494.

[Fen79] N. Fenichel, *Geometric singular perturbation theory*, J. Differential Equations, 31 (1979), pp. 53–98.

[FiH60] R. FitzHugh, *Thresholds and plateaus in the Hodgkin-Huxley nerve equations*, J. Gen. Physiol., 43 (1960), pp. 867–896.

[GS84] M. Golubitsky and D. Schaeffer, *Singularities and Groups in Bifurcation Theory*, Appl. Math. Sci. 51, Springer-Verlag, New York, 1984.

[GH04] J. Guckenheimer and R. Haiduc, *Canards at folded nodes*, Mosc. Math. J., (2004), to appear.

[GH83] J. Guckenheimer and P. Holmes, *Nonlinear Oscillations, Dynamical Systems and Bifurcations of Vector Fields*, Appl. Math. Sci. 42, Springer-Verlag, New York, 1983.

[HMM95] D. Hansel, G. Mato, and C. Meunier, *Synchrony in excitatory neural networks*, Neural Computation, 7 (1995), pp. 307–337.

[HH52] A. L. Hodgkin and A. F. Huxley, *A quantitative description of membrane current and its application to conduction and excitation in nerve*, J. Physiol. (London), 117 (1952), pp. 500–544.

[Jon95] C. K. R. T. Jones, *Geometric singular perturbation theory*, in Dynamical Systems, Lecture Notes in Math. 1609, Springer-Verlag, New York, 1995, pp. 44–120.

[KS01] M. Krupa and P. Szmolyan, *Extending geometric singular perturbation theory to nonhyperbolic points—fold and canard points in two dimensions*, SIAM J. Math. Anal., 33 (2001), pp. 286–314.

[Mel63] V. K. Melnikov, *On the stability of the center for time periodic perturbations*, Trans. Moscow Math. Soc., 12 (1963), pp. 1–57.

[MSLG98] A. Milik, P. Szmolyan, H. Löffelmann, and E. Gröller, *The geometry of mixed-mode oscillations in the* 3*d-autocatalator*, Internat. J. Bifur. Chaos Appl. Sci. Engrg., 8 (1998), pp. 505–519.

[MKKR94] E. F. Mishchenko, Yu. S. Kolesov, A. Yu. Kolesov, and N. Kh. Rhozov, *Asymptotic Methods in Singularly Perturbed Systems*, Monogr. Contemp. Math., Consultants Bureau, New York, 1994.

[Moe02] J. Moehlis, *Canards in a surface oxidation reaction*, J. Nonlinear Sci., 12 (2002), pp. 319–345.

[NAY62] J. S. Nagumo, S. Arimoto, and S. Yoshizawa, *An active pulse transmission line simulating nerve axon*, Proc. IRE, 50 (1962), pp. 2061–2070.

[PGS91] B. Peng, V. Gáspár, and K. Showalter, *False bifurcations in chemical systems: Canards*, Phil. Trans. Roy. Soc. London Sect. A, 337 (1991), pp. 275–289.

[PPS92] V. Petrov, S. K. Scott, and K. Showalter, *Mixed-mode oscillations in chemical systems*, J. Chem. Phys., 97 (1992), pp. 6191–6198.

[Rin85] J. Rinzel, *Excitation dynamics: Insights from simplified membrane models*, Fed. Proc., 44 (1985), pp. 2944–2946.

[RKZE03] H. G. Rotstein, N. Kopell, A. M. Zhabotinsky, and I. R. Epstein, *Canard phenomenon and localization of oscillations in the Belousov-Zhabotinsky reaction with global feedback*, J. Chem. Phys., 119 (2003), pp. 8824–8832.

[RT02] J. Rubin and D. Terman, *Geometric singular perturbation analysis of neuronal dynamics*, in Handbook of Dynamical Systems, Vol. 2, B. Fiedler, ed., North–Holland, Amsterdam, 2002, pp. 93–146.

[SK93] D. Somers and N. Kopell, *Rapid synchronization through fast threshold modulation*, Biol. Cybernet., 68 (1993), pp. 393–407.

[SW01] P. Szmolyan and M. Wechselberger, *Canards in* $\mathbb{R}^3$, J. Differential Equations, 177 (2001), pp. 419–453.

[Wec02] M. Wechselberger, *Extending Melnikov-theory to invariant manifolds on non-compact domains*, Dyn. Syst., 17 (2002), pp. 215–233.

[Wec98] M. Wechselberger, *Singularly Perturbed Folds and Canards in* $\mathbb{R}^3$, Thesis, Vienna University of Technology, Vienna, Austria, 1998.